

# Preprint

## Insights into Magma Storage Beneath a Frequently Erupting Arc Volcano (Villarrica, Chile) from Unsupervised Machine Learning Analysis of Mineral Compositions

Felix O. Boschetty<sup>1</sup>, David J. Ferguson<sup>1</sup>, Joaquín A. Cortés<sup>2</sup>, Eduardo Morgado<sup>3</sup>, Susanna K. Ebmeier<sup>1</sup>, Daniel J. Morgan<sup>1</sup>, Jorge E. Romero<sup>4</sup> and Carolina Silva Parejas<sup>5</sup>

<sup>1</sup>*Institute of Geophysics and Tectonics, School of Earth and Environment, University of Leeds, Leeds, UK*

<sup>2</sup>*Department of Geography & Geology, Edge Hill University, Ormskirk, UK*

<sup>3</sup>*Escuela de Geología, Universidad Mayor, Manuel Montt 367, Providencia, Santiago, Chile*

<sup>4</sup>*Department of Earth and Environmental Sciences, University of Manchester, Manchester, UK*

<sup>5</sup>*Escuela de Geología, Facultad de Ingeniería, Universidad Santo Tomás, Ejército Libertador 146, Santiago, Chile*

**The following document is a non-peer reviewed preprint uploaded on EarthArXiv. The manuscript has been submitted for publication in Geochemistry, Geophysics, Geosystems. Please note that the manuscript has not undergone peer-review and that subsequent versions of this paper may have slightly different content. If accepted, the final version will be available via a DOI link on this webpage. Please feel free to contact any of the authors, we welcome any feedback.**

1           **Insights into Magma Storage Beneath a Frequently**  
2           **Erupting Arc Volcano (Villarrica, Chile) from**  
3           **Unsupervised Machine Learning Analysis of Mineral**  
4           **Compositions**

5           **Felix O. Boschetty<sup>1</sup>, David J. Ferguson<sup>1</sup>, Joaquín A. Cortés<sup>2</sup>, Eduardo**  
6           **Morgado<sup>3</sup>, Susanna K. Ebmeier<sup>1</sup>, Daniel J. Morgan<sup>1</sup>, Jorge E. Romero<sup>4</sup>, and**  
7           **Carolina Silva Parejas<sup>5</sup>**

8           <sup>1</sup>Institute of Geophysics and Tectonics, School of Earth and Environment, University of Leeds, Leeds, UK

9           <sup>2</sup>Department of Geography & Geology, Edge Hill University, Ormskirk, UK

10           <sup>3</sup>Escuela de Geología, Universidad Mayor, Manuel Montt 367, Providencia, Santiago, Chile

11           <sup>4</sup>Department of Earth and Environmental Sciences, University of Manchester, Manchester, UK

12           <sup>5</sup>Escuela de Geología, Facultad de Ingeniería, Universidad Santo Tomás, Ejército Libertador 146,

13           Santiago, Chile

14           **Key Points:**

- 15           • Unsupervised machine learning reveals previously undetected compositional clus-
- 16           ters in Villarrica's crystal cargoes
- 17           • Thermodynamic models demonstrate magma storage occurs in a vertically exten-
- 18           sive system containing variably evolved mushy reservoirs
- 19           • Temporal trends in crystal cargo contents and mineral zoning suggest magma mix-
- 20           ing triggers unusual large mafic ignimbrites

21           Key words: Unsupervised Machine Learning, Crystal Cargoes, Thermodynamic Mod-

22           eling, Magma Mixing, Large Mafic Ignimbrites, Villarrica

---

Corresponding author: Felix O. Boschetty, [eefob@leeds.ac.uk](mailto:eefob@leeds.ac.uk)

**Abstract**

A key method to investigate magma dynamics is the analysis of the crystal cargoes carried by erupted magmas. These cargoes may comprise crystals that crystallize in different parts of the magmatic system (throughout the crust) and/or different times. While an individual eruption likely provides a partial view of the sub-volcanic plumbing system, compiling data from multiple eruptions builds a picture of the whole magmatic system. In this study we use machine learning techniques to analyze a large (>2000) compilation of mineral compositions from a highly active arc volcano: Villarrica, Chile. Villarrica's post-glacial eruptive activity (14 ka–present) displays large variation in eruptive style (mafic ignimbrites to Hawaiian effusive eruptions) yet its eruptive products have a near constant basalt-basaltic andesite bulk-rock composition. What therefore, is driving explosive eruptions at Villarrica and can differences in storage dynamics be related to eruptive style? We used hierarchical cluster analysis to detect previously unseen structure in olivine, plagioclase and clinopyroxene compositions, revealing the presence of compositionally distinct clusters. Using rhyolite-MELTS thermodynamic modeling we related these clusters to intensive magmatic variables: temperature, pressure, water content and oxygen fugacity. Our results provide evidence for the existence of multiple discrete (spatial and temporal) magma reservoirs beneath Villarrica where melts differentiate and mix with incoming more primitive magma. The compositional diversity of an erupted crystal cargo strongly correlates with eruptive intensity, and we postulate that mixing between primitive and differentiated magma drives explosive activity at Villarrica.

**Plain Language Summary**

Studies of volcanoes often focus on a single eruption. However, the magmatic systems beneath volcanoes are complex: magmas crystallize throughout the crust and the minerals erupted at the surface can be formed just prior to eruption, or thousands of years earlier. Here we use machine-learning methods to group mineral compositions from many eruptions of an active Chilean volcano to build a picture of the magmatic system. By using the appropriate mathematical treatment, we find that there are distinct groups of mineral compositions that were not identified by past studies. These different compositions are then used to demonstrate that different batches of magma have mixed throughout Villarrica's post-glacial history. This suggests that mixing of different magmas drives explosive eruptions at Villarrica volcano.

## 1 Introduction

Arc volcanoes produce most of the Earth’s subaerial volcanic activity and are responsible for some of the largest historical eruptions (Siebert et al., 2015). However the structure of the magmatic systems that feed these volcanoes is still largely unknown. The traditional view that the magmas erupted from arc volcanoes reside within a melt-dominated sub-volcanic ‘magma chamber’ has been superseded in recent years by a more nuanced view of magma storage and supply, whereby melts ascend through a vertically-extensive series of melt-rich zones, termed a ‘transcrustal magma system’ (TCMS, Cashman et al., 2017). This conceptual model describes the complex processing of primary magmas throughout the entire crust by crystallization, assimilation, and mixing (e.g., Annen et al., 2006, 2015). This combination of processes provides a theoretical framework to investigate the origins of the variety of mineral compositions and textures found in a single eruption’s crystal cargo.

Another recent advance in understanding magmatic systems is that crystal cargoes can be rapidly assembled from different parts of a magmatic system after protracted storage (e.g., Bergantz et al., 2015; Cooper & Kent, 2014; Mutch et al., 2019). Together with the TCMS model, they explain how a mineral assemblage erupted during a single event may contain: crystals formed from the carrier melt (autocrysts), crystals remobilized from other parts of the magmatic system (antecrysts), those from outside the magmatic system (xenocrysts), and crystals that form due to undercooling upon eruption (microlites) (Jerram & Martin, 2008). Therefore the crystal cargo of an eruptive deposit can be thought of as a snapshot of the underlying magmatic system. While an individual eruption likely provides a partial view of the sub-volcanic plumbing, compiling data from multiple eruptions can be used to build up a picture of the whole system. Building this complete picture requires well-characterized magmatic products from as many closely-spaced eruptions as possible.

Here we use established unsupervised machine learning techniques to analyze a large (>2000) compilation of mineral compositions from a highly active arc volcano: Villarrica, Southern Andes, Chile. We reveal previously unidentified structure in erupted mineral compositions and identify trends throughout Villarrica’s eruptive history related to crystal zoning and eruptive style. We utilize thermodynamic modeling to constrain the physical and chemical characteristics of Villarrica’s magmatic system to assess the suit-



87 ability of the TCMS model. Finally we discuss the role of magma mixing in driving ex-  
88 plosive behavior at Villarrica volcano, and the implications for future eruptions.

## 89 **2 Unsupervised Machine Learning Applied to Geochemical Data**

90 The term ‘unsupervised machine learning’ describes a class of algorithms that are  
91 designed to find patterns in multidimensional data. They are termed ‘unsupervised’ as  
92 they do not require any prior knowledge of the relationships between data. Unsupervised  
93 machine learning techniques can be used to gain insight into the structure of multivari-  
94 ate compositional data (data that describe quantity relative to a whole, i.e. close to a  
95 constant value such as 100%), which is common in geochemistry (e.g., Chiasera & Cortés,  
96 2011; X. Liu et al., 2020; Templ et al., 2008). The main advantage of these methods is  
97 that they allow the data to be interrogated in a multivariate sense and can highlight trends  
98 that otherwise would be difficult to identify using traditional Harker-style bi-variate plots  
99 (Cortés, 2009). Cluster analysis is an unsupervised machine learning technique that at-  
100 tempts to group data by some measure of similarity. The most similar data points are  
101 iteratively combined, until all data points belong to a single cluster. Hierarchical clus-  
102 ter analysis describes the relationship of all the data points to each other during this pro-  
103 cess, producing a hierarchy of data clusters organized by their similarity.

104 The majority of past studies that utilize cluster analysis have used it to character-  
105 ize the composition of volcanic products via analysis of whole-rock data sets, both for  
106 individual volcanoes (e.g., Mt Etna, Italy (Corsaro et al., 2013); Izu-Oshima, Japan (Kuritani  
107 et al., 2018)) and regional volcanism (e.g., the Virunga Volcanic Province (Barette et al.,  
108 2017)). Others have applied cluster analysis to individual phases from a single volcano  
109 e.g., silicate melt inclusions (Hamada et al., 2020); tephra glass (E. J. Liu et al., 2020);  
110 and minerals (Caricchi et al., 2020; Cortés et al., 2007). Some, but not all, of these stud-  
111 ies have recognized that compositional data require special mathematical treatment prior  
112 to analysis. In this study we use a log-ratio approach (i.e., Aitchison, 1986) to transform  
113 the compositional data into a compatible Euclidean geometry.

## 114 **3 Geological Background**

115 Villarrica (39.5°S, 71.9°W) is a Quaternary stratovolcano in the Andean volcanic  
116 arc, and part of the Chilean Central Southern Volcanic Zone (Figure 1a). The volcano

117 is Chile's most active, with more than 50 recorded eruptions since 1558 (Petit-Breuilh,  
118 2004), and is considered by the Chilean geological survey (SERNAGEOMIN), as the most  
119 hazardous of the 92 geologically active Chilean volcanoes (SERNAGEOMIN, 2019). Vil-  
120 larrica's post-glacial (14 ka–present) eruptive activity displays a wide range in eruptive  
121 intensity and magnitude. This includes two major eruptive events, that generated the  
122 Licán (ca. 13.9 ka BP) and Pucón (ca. 3.7 ka BP) mafic ignimbrites, with estimated vol-  
123 umes of 10 and 5 km<sup>3</sup> (non-DRE), respectively (Lohmar et al., 2012; Silva Parejas et al.,  
124 2010). In contrast, historic eruptions (1900–present) have ranged from Hawaiian to vi-  
125 olent Strombolian and are dominated by effusive lava flows (Pizarro et al., 2019). How-  
126 ever, the paroxysmal March 2015 eruption, which lasted just 30 minutes, was character-  
127 ized by a 1.5 km high fire fountain (Romero et al., 2018) and is the most recent demon-  
128 stration of Villarrica's explosive potential. Despite this variety in post-glacial eruptive  
129 style, Villarrica's volcanic products have a limited compositional range: 98% of the ju-  
130 venile whole-rock compositions collated in this study have 52–57 wt% SiO<sub>2</sub> (Figure 1).  
131 However, whole-rock data may not fully reflect the compositional variety of a magmatic  
132 system as heterogeneity may be present at a scale smaller than that of the whole rock  
133 sample (Pichavant et al., 2007). Therefore in this study, we focus on the main mineral  
134 phases erupted at Villarrica, whose compositions give insight into magma dynamics and  
135 the physical conditions of the magmatic system.

136 Typical Villarrica lavas and tephras are porphyritic with 10–15% modal crystals  
137 of mainly plagioclase feldspar and olivine, subordinate clinopyroxene, and small amounts  
138 of chromian spinel (Lohmar, 2008; Lohmar et al., 2012; Morgado et al., 2015; Pioli et  
139 al., 2015; Pizarro et al., 2019). Olivine crystals are usually euhedral to subhedral, often  
140 with resorbed rims. Clinopyroxene usually occurs as an unzoned subhedral phase, while  
141 plagioclase typically occurs as subhedral, reverse-zoned crystals with oxide inclusions,  
142 or as subhedral and unzoned crystals lacking inclusions. Groundmasses range from highly  
143 vesicular to highly crystalline, and are typically formed of plagioclase microlites and glass.

## 144 **4 Materials and Methods**

### 145 **4.1 Database Compilation**

146 We compiled a database of existing electron microprobe analyses of the most abun-  
147 dant mineral phases that are present in almost all of Villarrica's erupted products: olivine,

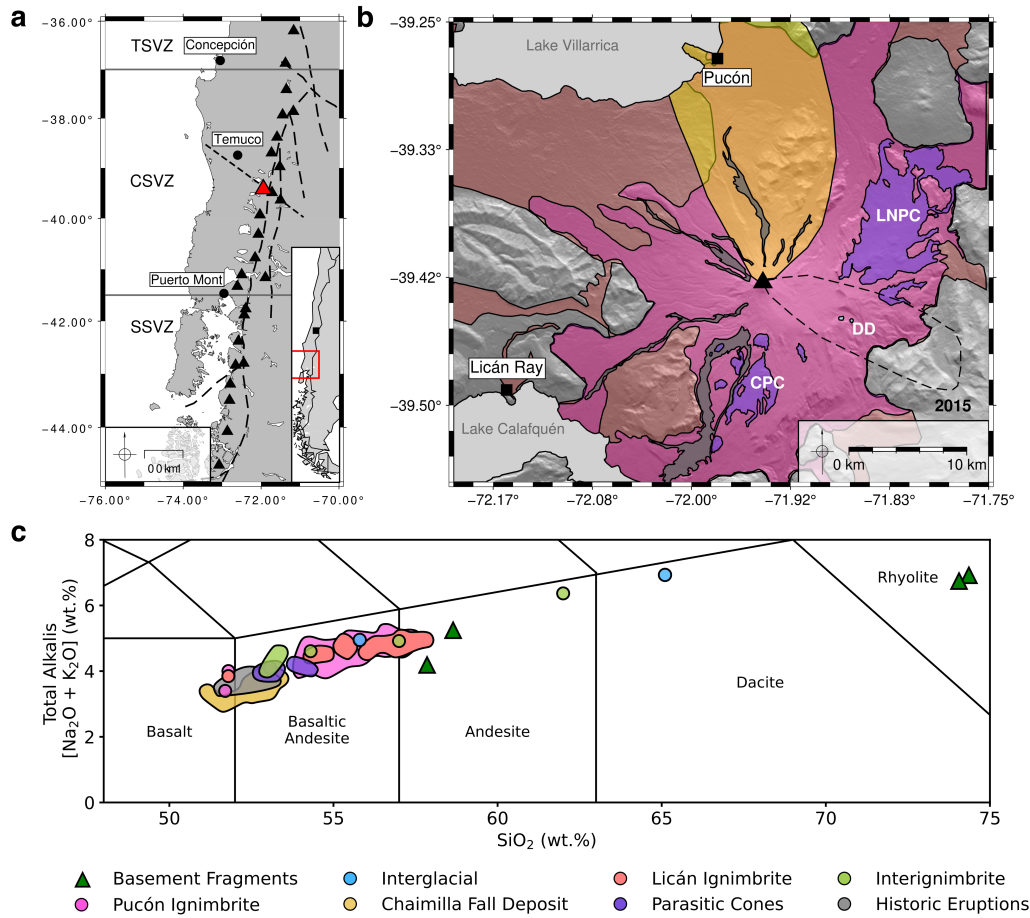


**Figure 1.** **a.** Map showing the location of Villarrica (red triangle) and other nearby active volcanoes (black triangles) in Chile's Southern Volcanic Zone (SVZ). The long-dashed black line is the Lliquiñe-Ofqui Fault Zone, short-dashed black line is the Mocho-Villarrica Fault Zone (Cembrano & Lara, 2009). TSVZ, Transitional South Volcanic Zone. CSVZ, Central South Volcanic Zone. SSVZ, Southern South Volcanic Zone (Stern, 2004). Inset shows the location of the CSVZ (red box) and the capital Santiago (black square). **b.** Simplified geological map (modified from Moreno and Clavero (2006)) showing the extent of key Villarrica eruptive deposits. The color of each deposit corresponds to the legend in 1c. LNPC, Los Nevados Parasitic Cones. CPC, Chaillupén Parasitic Cones. DD, Dacitic Domes. The location of the March 2015 tephra is shown by the black dashed line (Romero et al., 2018). **c.** Total-Alkali Silica (TAS Le Bas et al., 1986) diagram showing the bulk rock compositions of Villarrica eruptions and basement rocks from past studies (Clavero-Ribes, 1996; Hickey-Vargas et al., 1989, 2016; Lohmar, 2008; McGee et al., 2017; Morgado et al., 2015; Pioli et al., 2015; Pizarro et al., 2019; Silva Parejas, 2008; Wehrmann et al., 2014; Witter et al., 2004; Zajacz & Halter, 2007). This shows the homogeneous nature of Villarrica eruptive products: the vast majority of the juvenile products (98%) have 52–57 wt% SiO<sub>2</sub>.

148 plagioclase and clinopyroxene. These were sourced from published studies (Costantini  
149 et al., 2011; Morgado et al., 2015; Pioli et al., 2015; Pizarro et al., 2019; Wehrmann et  
150 al., 2014; Witter et al., 2004; Zajacz & Halter, 2009), theses (Clavero-Ribes, 1996; Lohmar,  
151 2008), and unpublished analyses. All data and their sources can be found in the Sup-  
152 plementary Material.

153 To ensure that only phases relevant to the magmatic system were considered, any  
154 analyses labeled as xenolith or microlite by the original authors were removed from the  
155 data sets. The analyses were then manually screened for errors e.g., misclassified, mixed-  
156 phase and poor-quality analyses. Any analysis without an analytical total between 98  
157 wt% and 102 wt% was removed. The cations per formula unit (cfu) were calculated for  
158 each mineral analysis based on stoichiometry, using 4, 32 and 6 oxygens for olivine, pla-  
159 gioclase and clinopyroxene, respectively. Total iron was assumed to be entirely FeO for  
160 plagioclase and olivine analyses. The method of Droop (1987) was used to calculate the  
161 proportion of Fe<sup>2+</sup> to Fe<sup>3+</sup> in clinopyroxene analyses. Clinopyroxene analyses with a to-  
162 tal cfu outside  $4.00 \pm 0.02$  were removed. After screening, 2277 analyses (out of an ini-  
163 tial 2611) were deemed suitable, these are broken down by eruption in Table 1.

## 164 **4.2 Data Quality and Limitations**

165 The database used in this study contains a large (>2200) total number of analy-  
166 ses, but the number of analyses per eruption is much smaller: only the 2015 eruption has  
167 nearly 100 analyses for either of the two most modally abundant minerals, olivine and  
168 plagioclase (Table 1). Therefore key compositional features of all the eruptions analyzed  
169 in this study might not have been detected: Cheng et al. (2017) suggests that 100 or more  
170 analyses are required to characterize the compositional and textural features of a min-  
171 eral population. Furthermore, all eruptive deposits have not been sampled and analyzed  
172 equally. Table 1 shows that there are a higher number of analyses of high-volume erup-  
173 tions (the Licán and Pucón ignimbrites), historic eruptions, and those with easily acces-  
174 sible deposits. The main route up Villarrica, the Pucón Ski Center Road, cuts both the  
175 Pucón ignimbrite and the Chaimilla Fall Deposit and provides easy access to historic erup-  
176 tions. Conversely, the Los Nevados and Chailupén parasitic cones, and the Dacitic Domes  
177 are further from established roads and tracks.

**Table 1.** Breakdown of Villarrica microprobe analyses included in the compiled database by eruption. Eruption stages are shown in italics where relevant. Eruptions are ordered from oldest to youngest. Radiometric ages and their source are shown where known.

Deposit	Age (years BP)	Ol	Plag	Cpx
Dacitic Dome	95,000 ± 15,000 <sup>a</sup>	11	20	8
Intraglacial Pyroclastic Deposit	40,000–14,000 <sup>a</sup>	3	9	8
Licán Ignimbrite	14,500–13,500 <sup>b,c</sup>			
<i>Initial Fall Deposit</i>		2	6	2
<i>Main Eruption</i>		19	85	49
Pucura Lava	>10,600 <sup>d</sup>	8	10	5
Afunalhue Pyroclastic Flow	4,090 <sup>d</sup>	5	2	8
Pre-Pucón Surge		3	14	10
Pre-Pucón Lava		6	12	3
Pucón Ignimbrite	3,510–3,710 <sup>e</sup>			
<i>Initial Fall Deposit</i>		6	8	5
<i>Unit 1</i>		27	31	32
<i>Unit 2</i>		28	56	34
<i>Unspecified</i>		25	56	42
Post-Pucón Lava		30	64	22
Chaimilla Fall Deposit	3,180 ± 40 <sup>f</sup>			
<i>Lower</i>		58	110	20
<i>Upper</i>		65	71	19
<i>Unspecified</i>		6	12	10
Los Nevados Cones	<2,600 & >2,600 <sup>a</sup>	25	42	26
Chaillupén Cones	<3,700 & >3,700 <sup>a</sup>	10	11	17
1921		42	91	54
1948		19	67	31
1963		4	0	0
1971		57	71	17
1984		16	54	0
1999		49	48	9
2000		43	79	0
March 2015		153	89	2
Unknown		6	0	0
Totals		726	1118	433

BP, Before Present. Ol, Olivine. Plag, Plagioclase. Cpx, Clinopyroxene. <sup>a</sup>Moreno and Clavero (2006). <sup>b</sup>Moreno (1993). <sup>c</sup>Clavero-Ribes (1996). <sup>d</sup>Lara and Clavero (2004). <sup>e</sup>Silva Parejas et al. (2010). <sup>f</sup>Costantini et al. (2011).

178 Additionally, there are likely systematic errors related to the different analytical  
 179 equipment in different labs, which are in turn calibrated with different standards. This  
 180 results in different analytical uncertainties for each of the past studies complicating di-  
 181 rect comparison. There is also little overlap between the eruptions sampled by different  
 182 studies. Without this, there is no way to quantify these systematic errors.

### 183 4.3 Compositional Data Constraints and the Log-Ratio Transformation

184 Compositional data carry only relative information, subject to non-negative and  
 185 constant-sum constraints (100 wt% etc.). These constraints mean that often used sta-  
 186 tistical methods that assume that data are normally distributed (i.e. unconstrained to  
 187 a constant value and varying from  $-\infty$  to  $+\infty$ ), are not directly applicable. In his sem-  
 188 inal work, Chayes (1971) established that it is the ratios between compositional data that  
 189 measure variability rather than absolute differences. To circumvent this problem, Aitchison  
 190 (1986) introduced several log-ratio transformations: linear transformations that map com-  
 191 positional data into an unconstrained Euclidean space.

192 There are several proposed log-ratio transformations: the additive log-ratio trans-  
 193 formation (Aitchison, 1986), the centered log-ratio transformation (Aitchison, 1986) and  
 194 the isometric log-ratio transformation (Egozcue et al., 2003). In this study, the mineral  
 195 data sets were transformed using the isometric log-ratio (*ilr*) transformation (equation  
 196 1), implemented using the Pyrolite python library (M. Williams et al., 2020). This trans-  
 197 formation was chosen as it ensures the transformed data have a non-singular covariance  
 198 matrix and preserves the geometric properties of the raw compositional data (Egozcue  
 199 et al., 2003):

$$200 \quad \textit{ilr}(x) = \sqrt{\frac{i}{i+1}} \ln \left[ \frac{g(x_1, \dots, x_i)}{x_{i+1}} \right], \quad i = 1, 2, \dots, D-1, \quad (1)$$

201 where,  $x$  is a compositional analysis,  $i$  is a specific part,  $D$  is the number of parts (el-  
 202 ements analyzed), and  $g(x_i)$  is the geometric mean of the parts of  $x$ :

$$203 \quad g(x_i) = \left( \prod_{i=1}^n x_i \right)^{\frac{1}{n}}. \quad (2)$$

204 A requirement of using any log-ratio transformation is that the data cannot con-  
 205 tain zeros (Cortés et al., 2007; Fry et al., 2000). Zeros in compositional data can be struc-  
 206 tural (e.g., K in clinopyroxene), below detection of the analytical technique, or simply

207 not analyzed (Fry et al., 2000). We removed structural zeros by only considering elements  
 208 that reasonably exist in a mineral’s structure. To deal with zeros resulting from detec-  
 209 tion limits, a detection limit of 0.05 wt% was assumed for all elements. The detection  
 210 limits were generalized because detection limits were not reported in all cases. Zeros re-  
 211 sulting from detection limits were replaced using the Multiplicative Replacement method  
 212 of Martín-Fernández et al. (2000) and Fry et al. (2000), which is equivalent to distribut-  
 213 ing a detection limit threshold evenly among the below detection zeros. Not all elements  
 214 (especially minor elements) were analyzed in every study. Elements that were measured  
 215 for less than half of each of the mineral data sets were not used in our analysis. A ta-  
 216 ble containing the elements used in cluster analysis for each of the mineral data sets can  
 217 be found in the Supplementary Material.

218 Variables with low abundances but high relative variances (often minor and trace  
 219 elements) have high log-ratio variances and therefore dominate any analysis of the com-  
 220 plete log-ratio transformed data set (Baxter et al., 2005; Greenacre & Lewi, 2009; Greenacre,  
 221 2019). To prevent this, we normalized the log-transformed data set using the column (part)  
 222 medians and standard deviations:

$$223 \quad X' = x'_{ij} = \frac{x_{ij} - \tilde{x}_i}{\sigma_i} \quad (3)$$

224 Where  $X'$  is the normalized data set,  $x_{ij}$  the  $i^{\text{th}}$  part of the  $j^{\text{th}}$  analysis,  $\tilde{x}_i$  is the col-  
 225 umn median, and  $\sigma_i$  is the column standard deviation. The median was chosen over the  
 226 arithmetic mean as the transformed data sets were non-normal: all four *ilr*-transformed  
 227 data sets failed the Henze-Zirkler multivariate normality test with a specificity of 0.05  
 228 (Henze & Zirkler, 1990). Relationships between the transformed compositional data were  
 229 then explored using hierarchical clustering methods over a Euclidean space.

#### 230 **4.4 Hierarchical Cluster Analysis**

231 Hierarchical clustering algorithms attempt to group data into clusters by some mea-  
 232 sure of similarity. Agglomerative clustering methods start by grouping the two most sim-  
 233 ilar data points into a cluster, then treating them as a single data point. The most sim-  
 234 ilar data points or clusters are then iteratively combined until only a single cluster con-  
 235 taining all the data remains. To cluster the data, a measure of dissimilarity (often called  
 236 distance) must be chosen. A popular measure is the Euclidean distance which is the equiv-

237 alent of Pythagoras’s Theorem but over more than two dimensions:

$$238 \quad d_E = \sqrt{\sum_{i=1}^n (x_i - y_i)^2} \quad (4)$$

239 Where  $d_E$  is the Euclidean distance matrix,  $i$  is the number of parts, and  $x$  and  $y$  are  
 240 the points considered. Next, a linkage method must be chosen, i.e. a method describ-  
 241 ing how the distances between points and clusters are used to relate them. We used ward  
 242 clustering (Ward, 1963), which minimizes the in-cluster variance, over alternatives such  
 243 as single-linkage or average-linkage as it doesn’t suffer from chaining (W. T. Williams  
 244 & Lambert, 1966; Wishart, 1969). The hierarchical clustering algorithm was implemented  
 245 using the scikit-learn python library (Pedregosa et al., 2011). Dendrograms depicting the  
 246 resultant hierarchy were used to determine a suitable number of clusters independently  
 247 for each mineral data set. This was chosen by drawing a horizontal line that cuts the tree  
 248 at the distance which has the largest separation between branches. This finds the num-  
 249 ber of clusters that maximizes inter-cluster separation. The dendrograms for the min-  
 250 eral data sets are shown in Figure 2.

#### 251 **4.5 Multivariate Outlier Detection**

252 Each cluster contained points normally distributed about its center, therefore out-  
 253 liers are, according to the empirical rule for normal distributions, those values located  
 254 at distances larger than three standard deviation from its center. To identify potential  
 255 outliers, the Mahalanobis distance, i.e. the distance of a given data point  $x$  and a dis-  
 256 tribution (Mahalanobis, 1936), was calculated for each cluster:

$$257 \quad D_M(\vec{x}) = \sqrt{(\vec{x} - \vec{\mu})^T C^{-1} (\vec{x} - \vec{\mu})} \quad (5)$$

258 where  $D_M$  is the Mahalanobis distance,  $\vec{x}$  is a matrix of data points in each cluster, and  
 259  $\vec{\mu}$  and  $C$  are the location and covariance estimators. The location and covariance esti-  
 260 mators were robustly calculated using the Minimum Covariance Determinant estimator  
 261 (MCD) (as in Filzmoser & Hron, 2008), implemented using the FastMCD algorithm (Rousseeuw  
 262 & Driessen, 1999) available in the scikit-learn python package (Pedregosa et al., 2011).  
 263 The Mahalanobis distances for each cluster can be approximated by a  $\chi^2$  distribution  
 264 (Rousseeuw & Zomeren, 1990). A critical Mahalanobis distance was determined for each



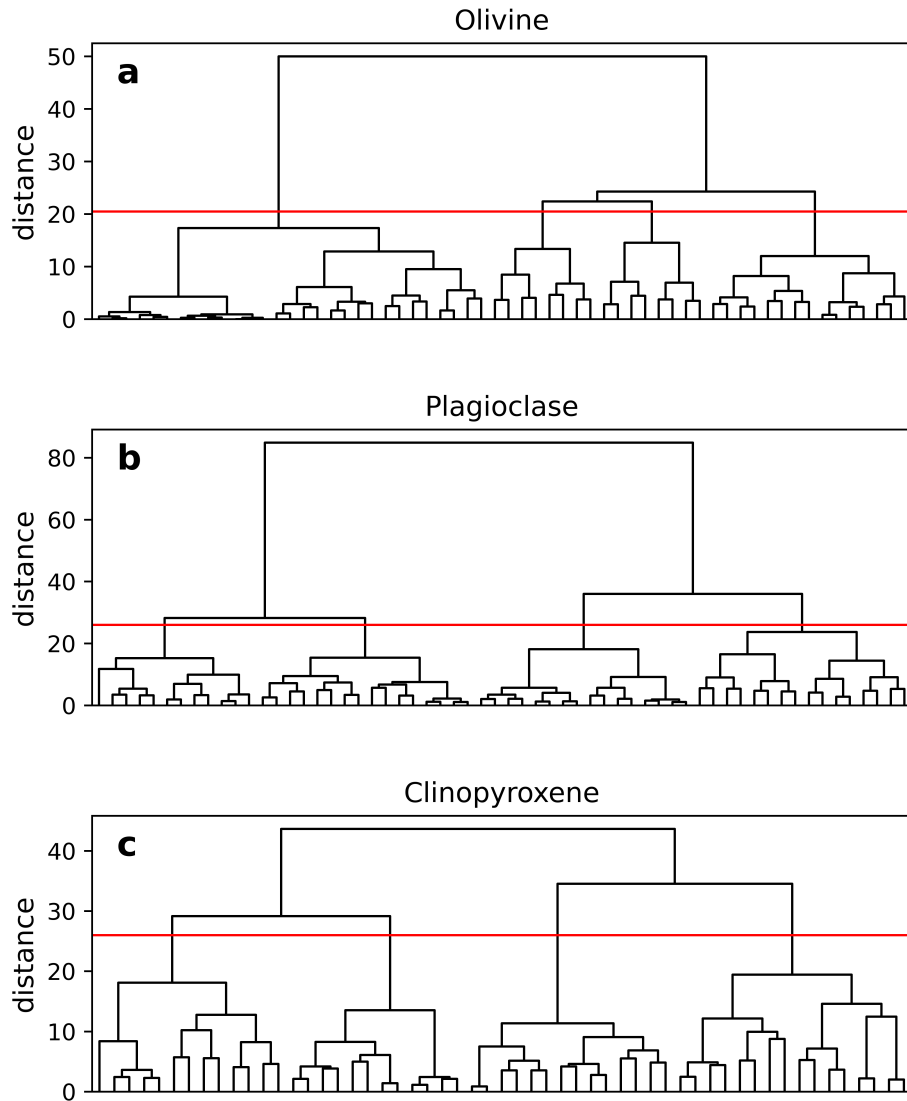


**Figure 2.** Dendrogram for each mineral data set, only the top five levels of each dendrogram are shown. The cutoff line which determines the number of clusters is shown by the red horizontal line.

265 cluster, above which a point is considered an outlier:

$$266 \quad D_M > (\chi_{p,1-\alpha}^2)^{1/2}, \quad (6)$$

267 which is the square root of the upper- $\alpha$  quartile of the  $\chi^2$  distribution with  $p$  degrees of  
 268 freedom, which were 5, 7, and 10 for olivine, plagioclase and clinopyroxene, respectively.  
 269 The typical choice for  $(1-\alpha)$  0.975 (Rousseeuw & Zomeren, 1990) was used i.e., the out-  
 270 liers will be contained in the upper 2.5% of the  $\chi^2$  distribution. Any identified outliers  
 271 were removed from the data sets.

#### 272 **4.6 Estimating Cluster Centers**

273 To characterize each of the identified clusters, a measure of central tendency is re-  
 274 quired. For compositional data, the best unbiased estimator of the expected value is de-  
 275 fined by the closed geometric mean (Cortés et al., 2007, and references within). To en-  
 276 sure that the center of the cluster is a valid mineral composition, the closed geometric  
 277 mean of each cluster was calculated, and the nearest (by Euclidean distance) data point  
 278 to each mean was used to represent each cluster.

#### 279 **4.7 Thermodynamic Modeling**

280 Thermodynamic modeling was carried out to investigate the likely provenance of  
 281 the identified mineral clusters with respect to the physical and chemical conditions of  
 282 magma evolution at Villarrica. We used the rhyolite-MELTS v1.2.0. algorithm (Ghiorso  
 283 & Gualda, 2015; Gualda et al., 2012), via the alphaMELTS 2.0 (originally *Adiabat\_1ph*  
 284 (Smith & Asimow, 2005)) front end, to model crystal fractionation from a primitive in-  
 285 put melt. The initial bulk composition of each model was estimated using the most prim-  
 286 itive glass composition reported at Villarrica: a post-entrapment-crystallization corrected,  
 287 olivine-hosted melt inclusion (VL15B-ol6-inc1, Mg# 68 at QFM+1) from an upper unit  
 288 of the Chaimilla fall deposit (Pioli et al., 2015). Isobaric fractional crystallization mod-  
 289 els were performed with temperature decreasing in 1°C increments from above the liq-  
 290 uidus, at a range of pressures (25, 50, 75 and 100 MPa and then increments of 100 up  
 291 to 700 MPa), variable initial water contents (0.0–6.0 wt% in increments of 0.5), and oxy-  
 292 gen fugacity buffers ( $fO_2$ ) QFM-0.5 (0.5 units below the Quartz-Fayalite-Magnetite buffer)

293 to QFM+2.25, in increments of 0.25. A total of 1560 rhyolite-MELTS simulations were  
 294 performed, one for each pressure, H<sub>2</sub>O and textitfO<sub>2</sub> permutation.

295 We quantified the goodness of fit of each rhyolite-MELTS simulation against each  
 296 of the representative mineral compositions, identified by cluster analysis, by calculating  
 297 the fit index (Gainsforth et al., 2015):

$$298 \quad FI = \sum_i \frac{|C_i^{model} - C_i^{rep}|}{C_i^{rep}} \quad (7)$$

299 Where  $FI$  is the fit index,  $C_i^{model}$  is the concentration of the  $i^{\text{th}}$  oxide in a mineral com-  
 300 position as calculated by rhyolite-MELTS and  $C_i^{rep}$  is the concentration of the  $i^{\text{th}}$  ox-  
 301 ide for the representative cluster composition being compared. All concentrations are  
 302 in wt% oxide. For olivine, the fit index was calculated using SiO<sub>2</sub>, MgO, FeO, CaO and  
 303 MnO concentrations. For plagioclase, SiO<sub>2</sub>, Al<sub>2</sub>O<sub>3</sub>, CaO and Na<sub>2</sub>O concentrations and  
 304 for clinopyroxene SiO<sub>2</sub>, Al<sub>2</sub>O<sub>3</sub>, FeO, MgO, and CaO. The best-fitting conditions were  
 305 found by calculating the minimum fit index for each representative composition. Temperature-  
 306  $fO_2$  heatmaps showing the fit index for every pressure-H<sub>2</sub>O combination and represen-  
 307 tative mineral composition can be found in the Supplementary Material.

## 308 5 Results

309 The compositions of minerals erupted in Villarrica’s crystal cargoes are diverse, es-  
 310 pecially in comparison to whole-rock compositions (Figure 1c). Olivine compositions range  
 311 from Fo<sub>50–87</sub>, plagioclase An<sub>50–96</sub>, and clinopyroxene Mg<sub>57–92</sub>. Despite this range in min-  
 312 eral compositions, hierarchical cluster analysis and outlier detection were performed suc-  
 313 cessfully on the three mineral data sets. Dendrograms (Figure 2) were used to find the  
 314 best number of clusters to represent each mineral data set. It is a coincidence that four  
 315 clusters best describe each mineral data set: there is no direct relationship between the  
 316 clusters identified in the different mineral types. For each of the identified clusters the  
 317 Mahalanobis distance was calculated and points that fall outside of a normal distribu-  
 318 tion identified and removed. This method detected 4, 11 and 22 outliers for olivine, pla-  
 319 gioclase and clinopyroxene, which corresponds to 0.6, 1.0 and 5.1% of each respective  
 320 data set. The representative compositions (centers) of each identified mineral cluster are  
 321 shown in Table 2.

**Table 2.** Representative compositions of each identified mineral cluster, given in wt% oxide and cations per formula unit. The concentration of FeO and Fe<sub>2</sub>O<sub>3</sub> in clinopyroxene was calculated with the method of Droop (1987). Clusters are ordered from most to least primitive.

Mineral Cluster	Olivine				Plagioclase				Clinopyroxene			
	Ol <sub>1</sub>	Ol <sub>2</sub>	Ol <sub>3</sub>	Ol <sub>4</sub>	Pl <sub>1</sub>	Pl <sub>2</sub>	Pl <sub>3</sub>	Pl <sub>4</sub>	Cpx <sub>1</sub>	Cpx <sub>2</sub>	Cpx <sub>3</sub>	Cpx <sub>4</sub>
SiO <sub>2</sub> (wt%)	39.67	39.00	38.23	37.91	45.60	47.66	52.78	55.54	51.51	49.85	51.83	51.29
TiO <sub>2</sub>									0.46	0.89	0.61	0.52
Al <sub>2</sub> O <sub>3</sub>					34.22	32.36	28.69	27.25	2.29	3.46	1.91	2.52
Cr <sub>2</sub> O <sub>3</sub>									0.49	0.08	b.d.	0.10
Fe <sub>2</sub> O <sub>3</sub>									1.56	2.76	2.23	0.00
FeO	15.57	21.50	22.49	25.65	0.48	0.61	0.87	0.55	6.07	7.34	8.18	8.75
MnO	0.24	0.33	0.36	0.48					0.20	0.30	0.43	0.22
MgO	45.21	39.20	38.62	35.74	0.08	0.10	0.18	0.05	16.88	14.79	14.98	14.59
CaO	0.18	0.28	0.20	0.27	18.49	16.35	12.73	10.00	19.04	19.52	20.04	19.93
Na <sub>2</sub> O					1.07	1.82	4.14	5.93	0.27	0.30	0.33	0.23
K <sub>2</sub> O					b.d.	0.05	0.14	0.13				
Si (mol)	0.990	1.006	0.997	1.002	10.250	10.659	11.422	11.896	1.918	1.869	1.922	1.938
Ti									0.130	0.025	0.017	0.015
Al					4.532	4.265	3.658	3.439	0.101	0.153	0.083	0.112
Cr									0.015	0.002	b.d.	0.003
Fe <sup>3+</sup>									0.043	0.078	0.062	0.000
Fe <sup>2+</sup>	0.325	0.464	0.490	0.567	0.090	0.114	0.158	0.099	0.189	0.230	0.254	0.276
Mn	0.005	0.007	0.008	0.011					0.060	0.010	0.014	0.007
Mg	1.682	1.507	1.501	1.408	0.027	0.033	0.059	0.016	0.937	0.827	0.828	0.822
Ca	0.005	0.008	0.006	0.008	4.453	3.918	2.951	2.295	0.759	0.784	0.796	0.807
Na					0.233	0.395	0.868	1.231	0.019	0.022	0.024	0.017
K					b.d.	0.007	0.020	0.018				
Fo (mol%)	83.81	76.46	75.39	71.29								
An					95.03	90.69	76.87	64.76				
Mg#									83.21	78.24	76.52	74.86

Blank cells denote elements not used in cluster analysis. b.d., below detection limit. -, not calculated. Fo, molar forsterite content. An, molar anorthite content. Mg#, magnesium number.

322 To visualize the distribution of the identified clusters and verify that they were com-  
 323 positionally distinct, two techniques were chosen to reduce the dimensionality of the *ilr*-  
 324 transformed data. First, principal component analysis (PCA) was performed and the re-  
 325 sulting first and second principal components plotted (Figure 3a-c). Then a t-distributed  
 326 Stochastic Neighbor Embedding (t-SNE) algorithm (Van der Maaten & Hinton, 2008)  
 327 was implemented with a perplexity value of 35. 10,000 iterations were used to ensure that  
 328 the projection was stable (Figure 3d-f). Both the PCA and t-SNE projections show that  
 329 the clusters identified by hierarchical cluster analysis are well-defined and have good sep-  
 330 aration. The distribution of outliers implies that outlier detection was successful: out-  
 331 liers are evenly distributed among the identified clusters and do not form clusters of their  
 332 own.

333 A major advantage of cluster analysis and the multivariate methods used in this  
 334 study, is that they allow patterns to be identified in multivariate space and reveal trends  
 335 that are hard to detect using bivariate plots. A good example of this is shown by the olivine  
 336 data set. Figure 4 shows probability density functions (PDFs) for each of the mineral  
 337 data sets and the identified clusters generated using Kernel Density Estimation (Silverman,  
 338 1986). The molar forsterite content ( $X_{Fo}=100 \cdot \text{Mg}/(\text{Mg}+\text{Fe}^{2+}+\text{Mn})$ ), molar anorthite  
 339 content ( $X_{An}=100 \cdot \text{Ca}/(\text{Ca}+\text{Na}+\text{K})$  in moles), and molar magnesium number  
 340 ( $\text{Mg}_{\#}=100 \cdot \text{Mg}/(\text{Mg}+\text{Fe}^{2+})$ ) were calculated, for olivine, plagioclase and clinopyroxene,  
 341 respectively. The resulting PDFs were multiplied by the number of data points in each  
 342 cluster, making them analogous to non-normalized histograms. The distribution of mo-  
 343 lar Fo for the complete olivine data set might suggest the existence of two clusters with  
 344 a Fo of 76 and 84. However cluster analysis, which considers the concentration of mul-  
 345 tiple elements (including minor elements), detects four clusters which could not be iden-  
 346 tified looking at the PDF of the complete data set alone. This demonstrates how clus-  
 347 ter analysis can identify and reveal otherwise hidden structure in mineral composition  
 348 data sets by detecting similarities in all elements analyzed.

349 Olivine compositions were successfully grouped into four clusters, whose cfu con-  
 350 tents show the expected proportionality with Fo (Table 2).  $\text{Fe}^{2+}$ , Si and Mn are all in-  
 351 versely proportional to Fo. However, Ca varies independently of Fo and the other ele-  
 352 ments, and therefore has potential to give insight into differing parental magma minor-  
 353 element compositions and/or differing  $\text{H}_2\text{O}$ -contents (Gavrilenko et al., 2016; Kamenet-  
 354 sky et al., 2006).

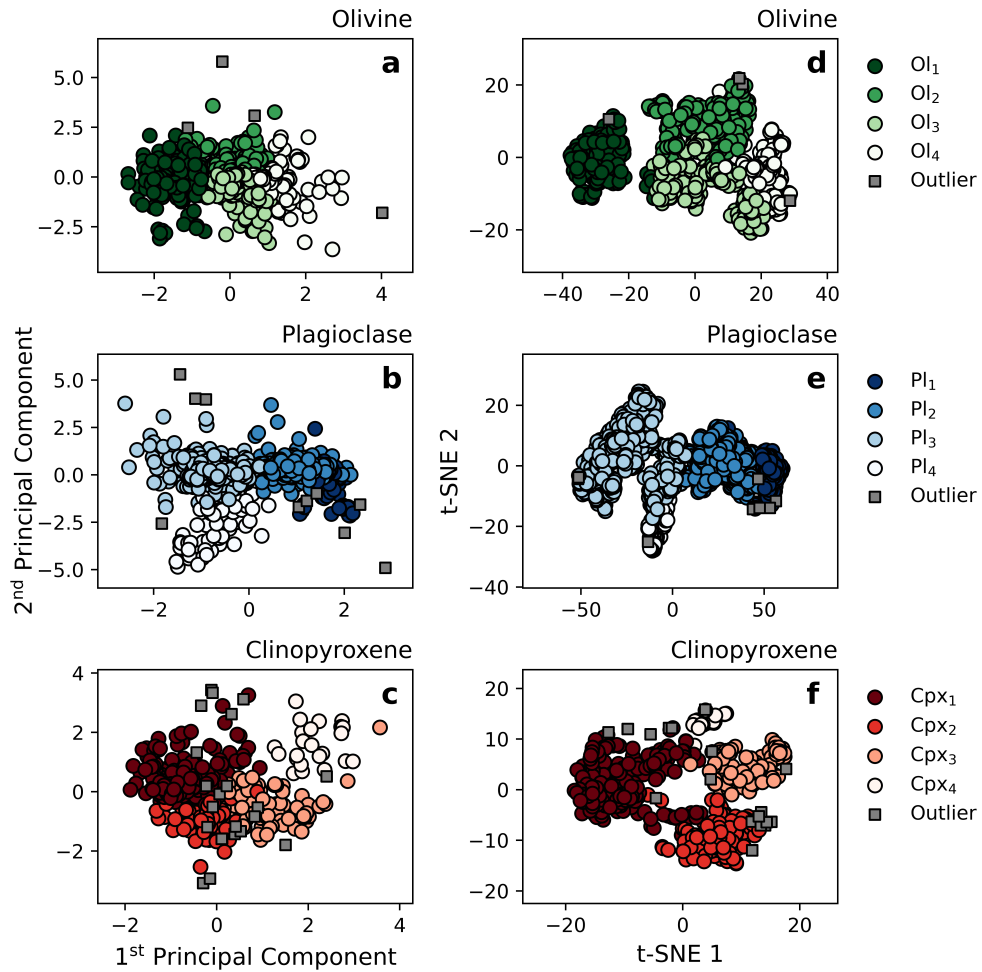


**Figure 3.** (a-c) Clustered data projected using the first and second principal components. (d-f) Clustered data projected using t-distributed stochastic neighborhood embedding (t-SNE) axes. Both projections show that the clusters identified by hierarchical clustering are well-defined.

355 Plagioclase compositions were grouped into four clusters. These show expected trends  
356 with increasing An-content: increasing Ca and Al; and decreasing Si, Na and K (Table  
357 2). However, Mg and Fe covary independently of the other elements and An-content. That  
358 they covary implies that the variations reflect one or more physical processes and are not  
359 due to the potentially high analytical uncertainties associated with Fe and Mg in plagioclase  
360 (Ginibre & Wörner, 2007). Variations in Fe and Mg in plagioclase independent  
361 of other elements, have been attributed to changes in Fe and Mg in the parental melt  
362 (Ginibre & Wörner, 2007; Singer et al., 1995), but might reflect melt-plagioclase dise-  
363 quilibrium caused by rapid growth (Ginibre & Wörner, 2007; Mollo et al., 2011; Singer  
364 et al., 1995).

365 Clinopyroxene compositions were also grouped into four clusters. However, the rep-  
366 resentative compositions show more complex trends than for plagioclase and olivine (Ta-  
367 ble 2). The identified clusters were characterized as follows: (1) a high-Cr and high-Mg<sub>#</sub>,  
368 (2) high-Al and high-Ti, (3) low-Al and low-Mg<sub>#</sub>, and (4) low-Fe<sup>3+</sup>. This might be the  
369 result of the higher-complexity of the clinopyroxene mineral structure, compared to feldspar  
370 and olivine. However, the identified clusters still appear to show some expected corre-  
371 lations with Mg<sub>#</sub>, with the most primitive Cpx<sub>1</sub> having the lowest incompatible elements,  
372 e.g., Mn and Ti, and Cpx<sub>3</sub> having higher incompatible elements and Ca. Cpx<sub>4</sub> has much  
373 lower calculated Fe<sup>3+</sup> content compared to the other three clusters which could reflect  
374 significantly different oxidation conditions during crystallization.

## 375 **5.1 Controls On Cluster Membership**

### 376 **5.1.1 Crystal Zoning**

377 Original studies classified each mineral analysis as unzoned, zoned – cores, inter-  
378 mediate, or rim. This information was not reported for a significant number of analy-  
379 ses (olivine: 20%, plagioclase: 32%, clinopyroxene: 35%), and there is no way to judge  
380 the accuracy of the designations. Therefore it was assumed that each of the source stud-  
381 ies categorized their analyses in the same manner. Figure 5 shows the proportion of crys-  
382 tal zones in each cluster for each category. There is no clear relationship between the clus-  
383 ter distribution and zoning for any of the three minerals.

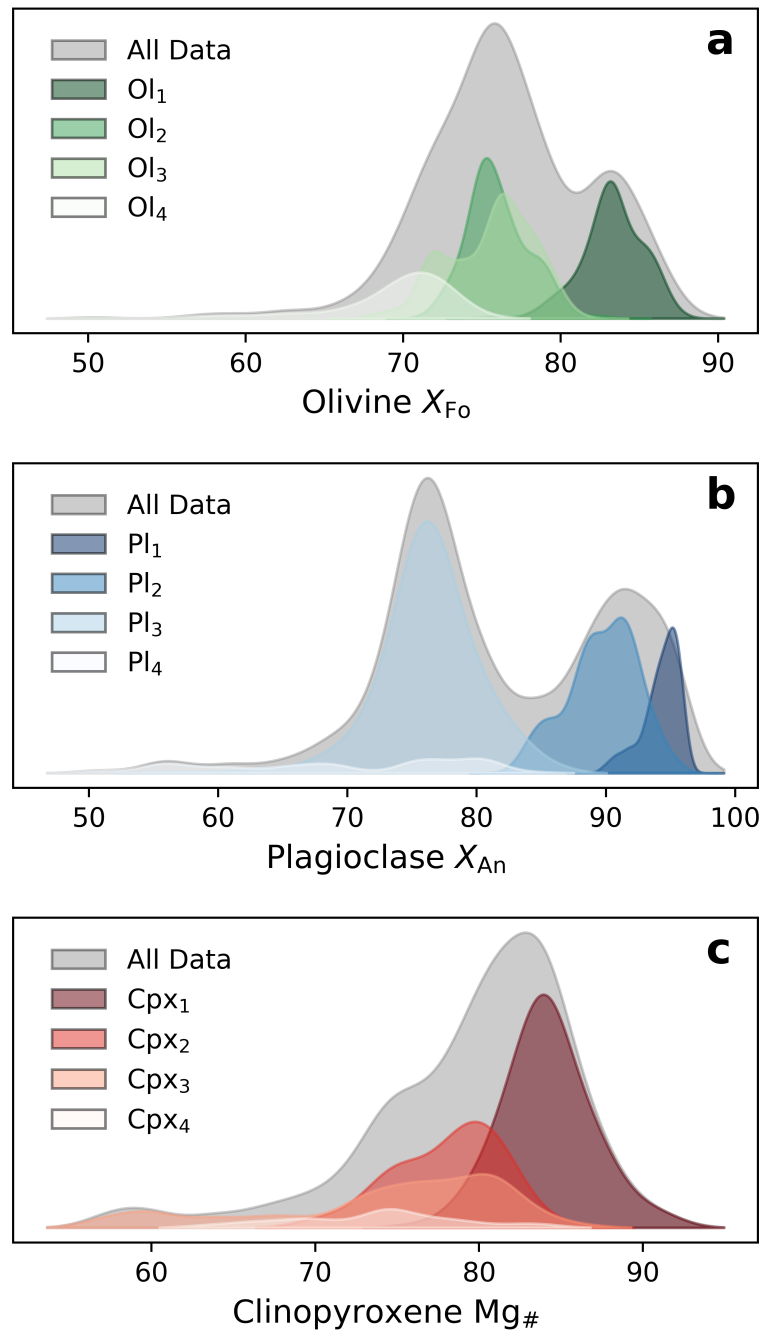


**Figure 4.** Plots of probability density functions (PDF) generated using Kernel Density Estimators (KDE) of each mineral subset and its clusters. Each PDF is scaled by the number of data points it was generated from, analogous to a histogram. Comparisons of the distribution of identified clusters with each respective complete data set highlights the ability of cluster analysis to identify otherwise hidden structure in mineral compositions.



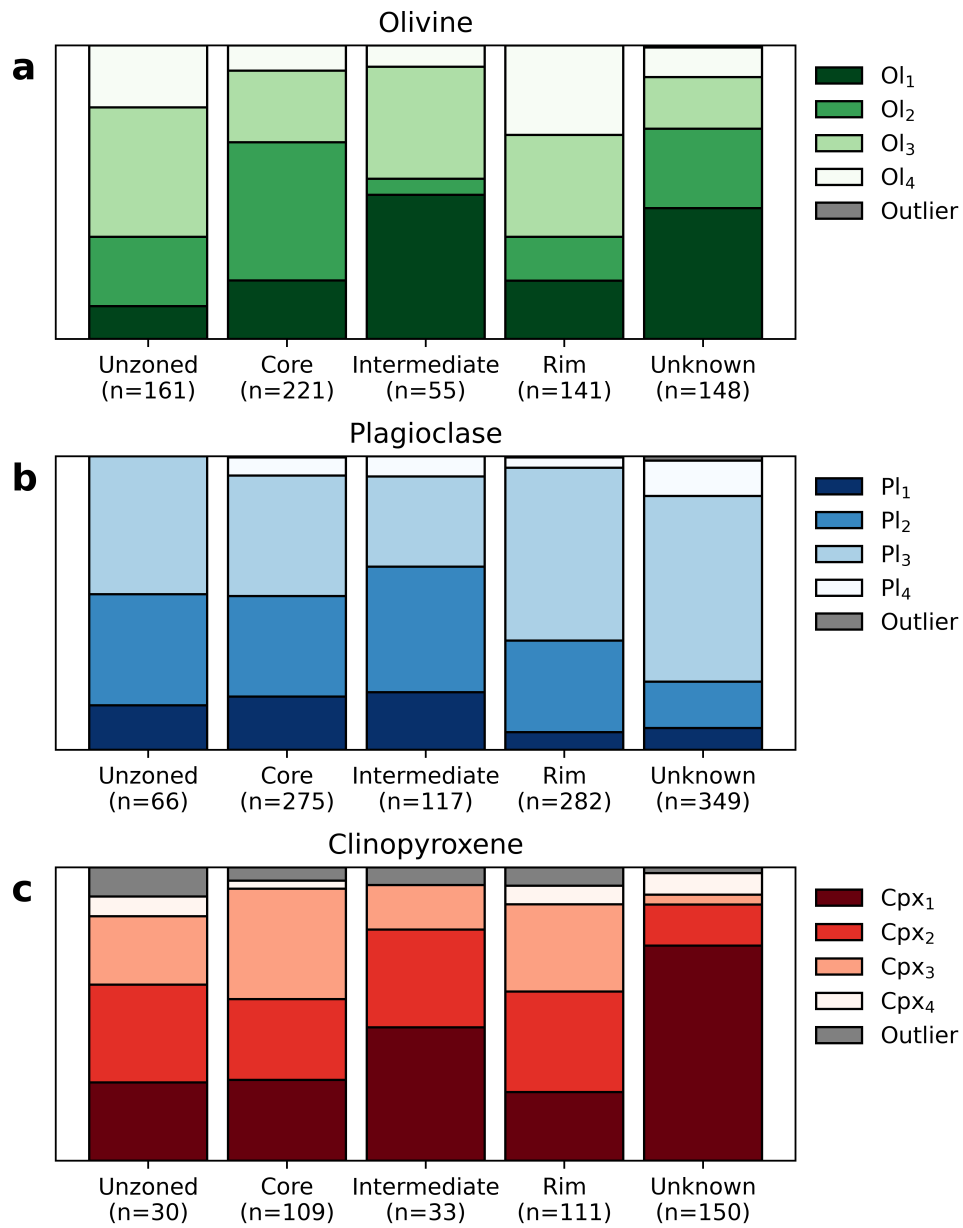


**Figure 5.** Stacked bar charts showing the effect of crystal zoning on cluster membership. The number of analyses in each category is shown in brackets. There is no clear pattern between cluster membership and crystal zoning.

384 **5.1.2 Eruption Age**

385 Figure 6 shows the proportion of phenocrysts from each cluster within individual  
 386 eruptive deposits sorted by age. There is a stark contrast between the composition of  
 387 crystal cargoes of historic eruptions (erupted in the last 100 years) and prehistoric erup-  
 388 tions (ca. 95–1.6 ka). Generally, the crystal cargoes of historic eruptions contain a smaller  
 389 variety of crystal compositions. This is especially pronounced for feldspar and clinopy-  
 390 roxene compositions (Figure 6b,c). Both feldspar and clinopyroxene compositions be-  
 391 come markedly more homogeneous through to the present day: erupted plagioclase com-  
 392 positions are dominated by  $Pl_3$  and erupted clinopyroxene compositions are dominated  
 393 by  $Cpx_1$ . Generally, historic eruptions contain a higher proportion of  $Ol_2$  than prehis-  
 394 toric eruptions, but olivine compositions are more variable than plagioclase and clinopy-  
 395 roxene (Figure 6).

396 Of the three minerals analyzed in this study, olivine cluster proportions vary the  
 397 most from eruption to eruption. For example, the Licán ignimbrite has a large propor-  
 398 tion of primitive olivine ( $Ol_1$ ) whereas the Pucón ignimbrite is made up almost entirely  
 399 of more evolved olivine ( $Ol_3$  and  $Ol_4$ ). The historic eruptions are dominated by more  
 400 evolved olivine ( $Ol_2$  and  $Ol_3$ ). However, the March 2015 eruption is distinct from the  
 401 other historic eruptions, as it has large proportion of all four olivine clusters. Therefore  
 402 the olivine cluster proportions of the 2015 eruption is more similar to the prehistoric,  
 403 than the other historic eruptions.

404 The proportion of plagioclase clusters varies widely between the historic and pre-  
 405 historic eruptions. Generally, the prehistoric eruptions contain a greater variety of pla-  
 406 gioclase compositions: the Licán and Pucón ignimbrites are the only to contain all four  
 407 plagioclase clusters. The most evolved plagioclase cluster ( $Pl_4$ ) only occurs in the three  
 408 oldest eruptions: the Dacitic Dome, and the Licán and Pucón ignimbrites. The most prim-  
 409 itive plagioclase ( $Pl_1$ ) is restricted almost entirely to prehistoric eruptions. In contrast,  
 410 the crystal cargoes of the historic eruptions are dominated by the intermediate  $Pl_3$ , whose  
 411 proportion increases through time from the 1921 through to the March 2015 eruption.

412 Clinopyroxene cluster membership broadly corresponds to that of olivine and pla-  
 413 gioclase: the greatest amount of variation is present in the oldest eruptions. Clinopy-  
 414 roxene becomes scarcer and more compositionally homogeneous in later eruptions: clus-  
 415 ter  $Cpx_2$  and  $Cpx_3$  are most dominant in the prehistoric eruptions while  $Cpx_1$  is much

416 more dominant in the historic eruptions. Very little to no clinopyroxene was erupted af-  
417 ter the 1948 eruption.

### 418 **5.1.3 Eruptive Center Location**

419 Villarrica's flanks host over 30 parasitic or adventitious cones which form two groups:  
420 the Los Nevados group to the northeast and the Chaillupén group to the south (Moreno  
421 & Clavero, 2006) (Figure 1b). Other than the scoria and lavas of these two groups of cones,  
422 all other eruptive deposits are thought to originate from Villarrica's main vent, although  
423 the location of this main vent has changed through time (Moreno & Clavero, 2006). The  
424 cluster membership for the two groups of parasitic cones are shown in Figure 6 (labeled  
425 LNPC and CPC, respectively). The proportion of phenocrysts in each cluster for the two  
426 groups of cones are distinct. For example, the Chaillupén cones contain the most prim-  
427 itive olivine ( $Ol_1$ ) and the most evolved clinopyroxene ( $Cpx_4$ ), unlike the Los Nevados  
428 cones. This might be because the two sets of cones tap different parts of Villarrica's mag-  
429 matic system, or they sample the system at different points in time. Compared to the  
430 eruptions from the central vent, the two sets of parasitic cones are more diverse than the  
431 historic eruptions, and most similar to the prehistoric eruptions. This is especially ap-  
432 parent when comparing the olivine and clinopyroxene cluster memberships. More detailed  
433 studies of the two groups of cones are needed to constrain their ages and their petrol-  
434 ological differences to each other and products from the main vent (e.g., Robidoux et al.,  
435 2021).

### 436 **5.1.4 Eruption Volume and Intensity**

437 Villarrica's post-glacial eruptions show large variation in volume and intensity, most  
438 notable are the differences between the explosive high-volume mafic ignimbrites (Licán  
439 and Pucón) with the smaller-volume comparatively-effusive historic eruptions. The large  
440 volume of the ignimbrites and association with caldera collapse suggests that a large pro-  
441 portion of Villarrica's magmatic system was evacuated during those eruptions. This might  
442 be expected to produce products with a higher compositional variety, e.g., both evolved  
443 and primitive compositions, especially if the magmatic system were to contain multiple  
444 somewhat isolated bodies that evolved independently. This is indeed reflected in the clus-  
445 ter memberships of the historic versus older eruptions. Generally, the more explosive,  
446 older eruptions have a higher diversity in mineral compositions, especially the Licán and

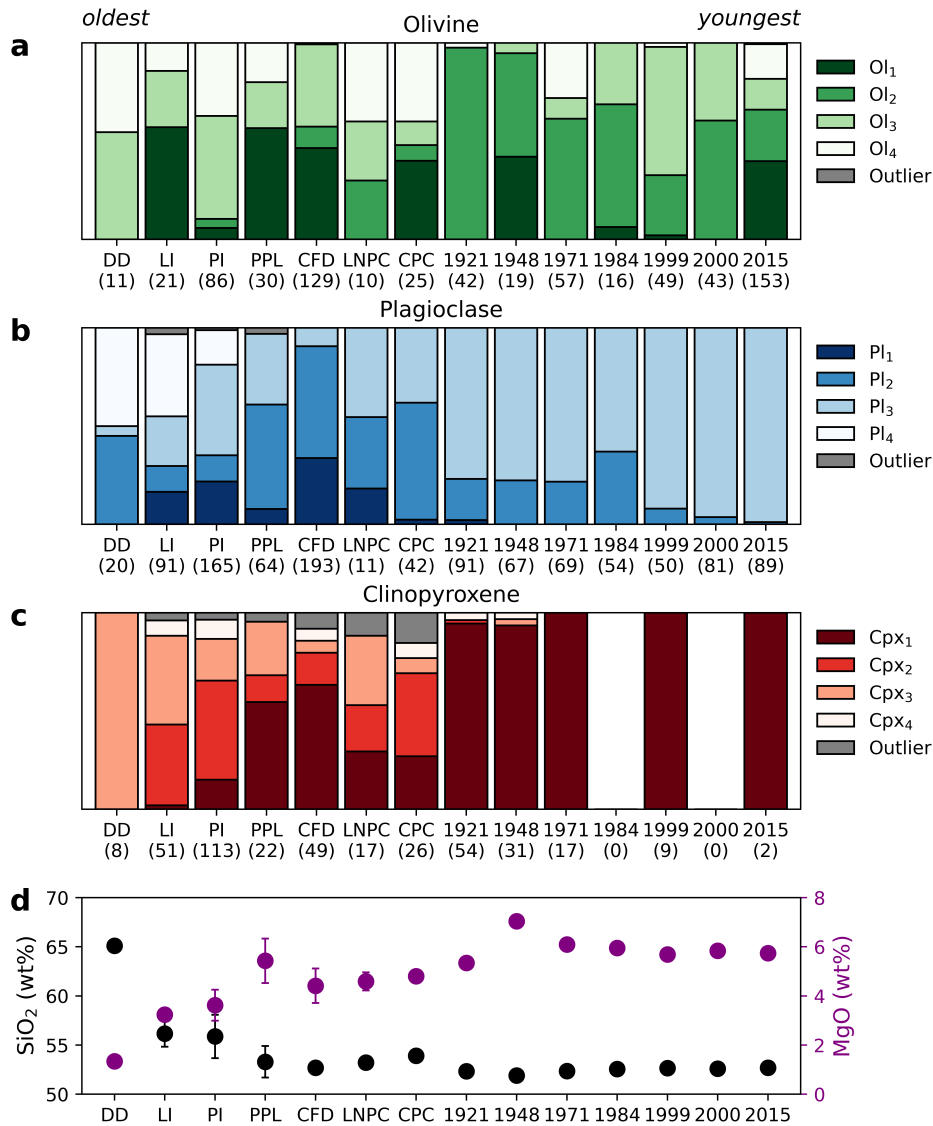


**Figure 6.** (a-c) Stacked bar charts showing the cluster membership of the different eruptions sorted by age. The number of analyses for each eruption are shown in brackets. Only those eruptions with more than 10 phenocryst compositions are shown. DD, Dacitic Dome. LI, Licán Ignimbrite. PI, Pucón Ignimbrite. PPL, Post-Pucón Lava. CFD, Chaimilla Fall Deposit. LNPC, Los Nevados Parasitic Cones. CPC, Chillupén Parasitic Cones. Historic eruptions are labeled by eruption year. (d) Plot of mean whole-rock SiO<sub>2</sub> and MgO contents. Error bars show  $\pm 1$  standard deviation. Whole-rock data sources are the same as in Figure 1c.

**Table 3.** The best fitting conditions for each identified mineral cluster from rhyolite-MELTS thermodynamic modeling. Oxygen fugacity is shown in log units relative to the QMF buffer.

Mineral	Cluster	T (°C)	P (MPa)	$\Delta f_{O_2}$	H <sub>2</sub> O (wt%)	Min FI
Olivine	Ol <sub>1</sub>	1041	300	1.00	5.5	0.202
	Ol <sub>2</sub>	1047	200	-0.25	3.5	0.063
	Ol <sub>3</sub>	1039	400	0.25	4.0	0.065
	Ol <sub>4</sub>	1042	200	-0.50	2.5	0.035
Plagioclase	Pl <sub>1</sub>	1020	200	-0.50	5.0	0.843
	Pl <sub>2</sub>	1016	200	-0.50	5.0	0.113
	Pl <sub>3</sub>	1039	25	1.25	5.5	0.108
	Pl <sub>4</sub>	967	600	1.75	3.0	0.040
Clinopyroxene	Cpx <sub>1</sub>	1041	100	2.00	0.0	0.083
	Cpx <sub>2</sub>	985	50	0.75	1.5	0.061
	Cpx <sub>3</sub>	1011	25	1.25	0.0	0.079
	Cpx <sub>4</sub>	970	25	0.75	0.5	0.037

T, temperature. P, pressure. Min FI, minimum fit index calculated for each mineral using equation 7.

447 Pucón ignimbrites. Of the historic eruptions the intense March 2015 eruption, that pro-  
 448 duced a 1.5 km high fire fountain, erupted more diverse olivine compositions than any  
 449 other historic eruption.

## 450 5.2 Thermodynamic Modeling

451 The representative compositions identified by hierarchical clustering were well re-  
 452 produced by the relatively simple model set up, shown by the low minimum fit indexes  
 453 (Table 3). However, the most primitive clusters (Ol<sub>1</sub> and Pl<sub>1</sub>) have higher minimum fit  
 454 indexes than the other olivine and plagioclase clusters. This suggests that the initial bulk  
 455 composition used, the most primitive melt inclusion found at Villarrica, was not suffi-  
 456 ciently primitive to reproduce exactly these compositions. However the calculated fit in-  
 457 dexes are not so different as to suggest that the models do not provide a reasonable in-  
 458 dication of the conditions of crystallization.

459 The best fitting pressure and temperature conditions from the rhyolite-MELTS sim-  
 460 ulations broadly agree with thermobarometry results from past studies (Figure 7). Pres-  
 461 sures from both simulations and past thermobarometry show that polybaric crystalliza-  
 462 tion, extending to at least the mid to lower crust (ca. 600 MPa), is required to produce  
 463 the variety of erupted mineral compositions at Villarrica. The predicted temperatures  
 464 from rhyolite-MELTS (950-1100°C) are less than those calculated by thermobarometry

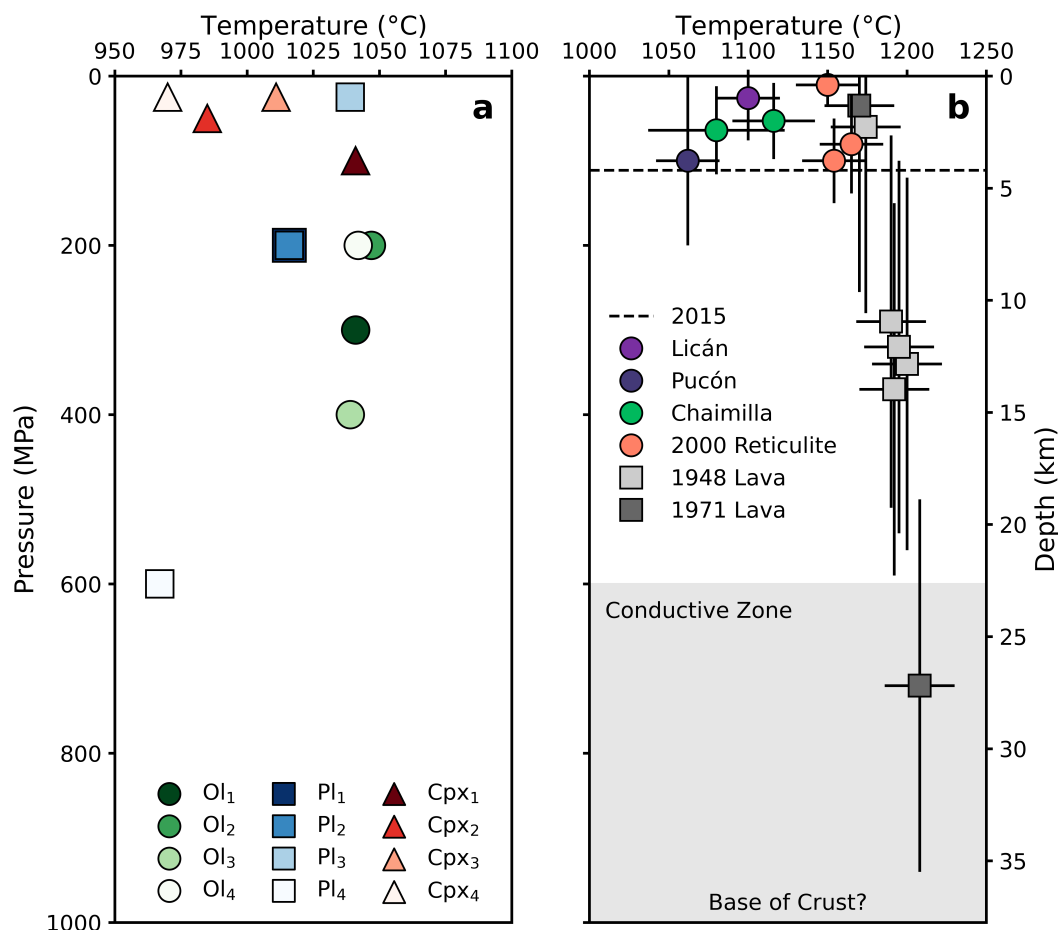


**Figure 7.** **a.** Best fitting temperature and pressures from rhyolite-MELTS simulations for each of the identified mineral clusters. **b.** Pressure-temperature plot of geothermobarometry results from past studies of Villarrica (Lohmar, 2008; Lohmar et al., 2012; Morgado et al., 2015; Pioli et al., 2015; Pizarro et al., 2019; Witter et al., 2004). The error bars correspond to the range of uncertainty for each result. The corresponding depth is calculated assuming a constant density of  $2.7 \text{ g cm}^{-3}$ . The black dotted line is the calculated depth (ca. 4.2 km) of the deformation source for the March 2015 eruption (Delgado et al., 2017). The gray shading corresponds to an area of high conductivity (ca. 19-50 km) (Kapinos et al., 2016).

465 (1050–1250°C). This discrepancy is likely due to the high (>2 wt%) water contents of  
 466 majority of the best fitting rhyolite-MELTS simulations: the olivine-augite geothermome-  
 467 ter which was used in the past studies was not calibrated on experiments with high wa-  
 468 ter contents, and therefore overestimated temperatures (Loucks, 1996).

469 The most primitive olivine (Ol<sub>1</sub>) formed at relatively high temperatures and pres-  
 470 sures (1041 °C, 300 MPa). Furthermore, Ol<sub>1</sub> has both the highest  $f\text{O}_2$  and water con-  
 471 tent (QFM+1.00, 5.5 wt%). This is in agreement with experimental and natural stud-

472 ies of olivine crystallization from basaltic melts (Feig et al., 2010; Gavrilenko et al., 2016).  
473 This suggests that it formed from relatively primitive undegassed melts with a relatively  
474 low residence time in the crust prior to crystallization. In contrast, the most evolved olivine  
475 cluster (Ol<sub>4</sub>) has a lower pressure,  $fO_2$ , and water content. The two most primitive pla-  
476 gioclase clusters (Pl<sub>1</sub> & Pl<sub>2</sub>) have high water contents (5.0 wt%) and relatively high tem-  
477 peratures (1020 and 1016 °C), as expected from experimental studies (Panjasawatwong  
478 et al., 1995; Takagi et al., 2005; Waters & Lange, 2015). In contrast, the most evolved  
479 plagioclase (Pl<sub>4</sub>) has a significantly lower crystallization temperature (967 °C), and a no-  
480 tably higher pressure and  $fO_2$  (600 MPa, QFM+1.75). All representative clinopyrox-  
481 ene compositions are best fit at lower pressures (25–100 MPa), and at a variety of tem-  
482 peratures (970–1041°C) and water contents (0–1.5 wt%).

## 483 **6 Discussion**

### 484 **6.1 Vertically and Laterally Extensive Magma Processing**

485 Several models of volcanic systems that integrate geophysical, geochemical, and petro-  
486 logical information have concluded that magma processing beneath arc volcanoes likely  
487 takes place throughout the crust in trans-crustal magma systems (Annen et al., 2006,  
488 2015; Cashman et al., 2017; Hildreth & Moorbath, 1988). There are multiple lines of ev-  
489 idence that suggest that this is the case at Villarrica volcano. We have compared rep-  
490 resentative mineral compositions identified via clustering, with thermodynamic fractional  
491 crystallization models of a simple Villarrica-like system. The comparisons suggest that  
492 polybaric crystallization, at pressures up to 600 MPa, are required to produce the min-  
493 eral compositions erupted at Villarrica (Figure 7a). This is supported by thermobarom-  
494 etry from past studies that focused on individual eruptions (Figure 7b). The majority  
495 of pressures calculated from thermobarometry are in the shallow crust (0–150 MPa), but  
496 pressures calculated from olivine-augite pairs erupted during historic eruptions extend  
497 to 700 MPa. Additionally, Kapinos et al. (2016) detected a low conductivity zone be-  
498 neath Villarrica volcano that extends from 19–50 km, beyond the base of the crust.

499 As well as vertical connectivity, there is also evidence of lateral connectivity within  
500 Villarrica’s magmatic system (e.g., Ebmeier et al., 2018; Lerner et al., 2020) (Figure S1).  
501 Nested calderas, kilometers in diameter, were produced during large eruptions at Vil-  
502 larrica and surround the current central vent: Caldera 1 (ca. 100ka), Caldera 2 (ca. 14ka),

503 and Caldera 3 (ca. 3.7ka) (Moreno & Clavero, 2006). Calderas 1 and 2 cover an area of  
504 6.5 by 4.2 km (long axes), Caldera 3 is roughly circular and 2 km in diameter. After the  
505 March 2015 eruption, Delgado et al. (2017) detected reinflation (4.2 km deep) of part  
506 of Villarrica's magmatic system, ca. 5 km SE of the central vent near the edge of Calderas  
507 1 and 2. Further afield still, are the two groups of parasitic cones on Villarrica's flanks.  
508 The Los Nevados group contain fissures and cones that extend to ca. 10 km to the NE  
509 and the Chaillupén group extend ca. 12 km to the south of the present central vent. Re-  
510 cently Pavez et al. (2020) detected a low conductivity zone (ca. 4 km deep) associated  
511 with the Los Nevados group. Combined, all these lines of evidence demonstrate that Vil-  
512 larrica's magmatic system is spatially extensive and imply that different parts of the sys-  
513 tem are tapped to accumulate the crystal cargo of each eruption.

## 514 **6.2 The Role of Magma Mixing**

515 The compositional variety observed within crystal cargoes erupted, combined with  
516 evidence for spatially extensive magma processing, suggest that Villarrica's magmatic  
517 system comprises multiple, variably-evolved reservoirs distributed throughout the crust.  
518 This is supported by widely varying best fitting intensive variables from Rhyolite-MELTS  
519 thermodynamic simulations (Table 3). In addition to the range of best-fit pressures, there  
520 is a large range of best fitting crystallization temperatures that reproduce crystal com-  
521 positions (967–1047°C). There is also a large variation in best-fitting water contents from  
522 anhydrous to 5.5 wt%. This implies that degassing plays a large role in driving crystal-  
523 lization in Villarrica's magmatic system, as has been suggested for other arc volcanoes  
524 (e.g., Bouvet de Maisonneuve et al., 2012; Blundy et al., 2006). The large range of best  
525 fitting  $fO_2$  values (-0.5–2.00  $\Delta QFM$ ) suggests that crystallization is occurring from melt  
526 that has undergone different amounts of degassing, fractional crystallization, and/or mix-  
527 ing (Carmichael, 1991; Lindsley & Frost, 1992; Sato, 1978). Together these results im-  
528 ply that reservoirs that are infrequently disturbed by ascending primitive magma, cool  
529 and differentiate via fractional crystallization to produce evolved crystal compositions  
530 e.g.,  $Pl_4$  ( $An_{62}$ ). Prior to eruption, ascending primitive melt interacts with multiple reser-  
531 voir. This mixing of magmas with different compositions produces new compositions  
532 which may be recorded in zoned crystals (Figure 5). These antecrysts are accumulated  
533 as melts ascend resulting in the variety of erupted mineral compositions in a single crys-  
534 tal cargo (Figure 6).



535 The important role of magma mixing at Villarrica is supported by our observation  
536 that the proportion of identified clusters do not show clear trends when they are com-  
537 pared to crystal zoning (Figure 5). If fractional crystallization is the dominant process  
538 during magma processing in Villarrica’s magmatic system, we would expect mineral cores  
539 to be dominated by primitive compositions and rims by more evolved compositions. How-  
540 ever, both primitive and evolved clusters are present as cores, intermediate, and rim zones  
541 of all three of the commonly erupted minerals. This implies that magma mixing plays  
542 a role in assembling crystal cargoes at Villarrica (e.g., Ruprecht et al., 2012; Streck, 2008)

543 Furthermore, textural evidence for magma mixing is present in almost all Villar-  
544 rica’s eruptive deposits. The Dacitic Dome contains reverse and oscillatory-zoned pla-  
545 gioclase, olivine with fayalitic rims ( $\text{Fo}_{58}$ ) and reverse-zoned clinopyroxene (Lohmar, 2008).  
546 The Licán ignimbrite has both reverse and oscillatory-zoned plagioclase, reverse-zoned  
547 clinopyroxene, and orthopyroxene rims surrounding olivine crystals (Lohmar et al., 2012).  
548 A pre-Pucón surge deposit contains banded pumice, the pale bands have a bulk  $\text{SiO}_2$  of  
549 63 wt% (Moreno et al., 1994; Lohmar, 2008). The Pucón ignimbrite contains plagioclase  
550 crystals with resorbed cores and rims, sieve textures, and low-An microlites. Clinopy-  
551 roxene is often reverse-zoned (Lohmar, 2008). Additionally, what is thought to be a dacitic  
552 enclave in a scoria bomb of the Pucón ignimbrite has been observed (McCurry & Schmidt,  
553 2001; McCurry et al., 2004). The Chaimilla Fall Deposit contains complexly zoned pla-  
554 gioclase crystals with both reverse rims and widespread evidence of resorption (Pioli et  
555 al., 2015). Multiple historic eruptions also contain similar indicators: An-poor plagio-  
556 clase is present as both rims of oscillatory-zoned crystals and crystals with resorption  
557 textures. Both olivine and clinopyroxene crystals display resorption textures (Morgado  
558 et al., 2015; Pizarro et al., 2019).

559 The ubiquity of evidence for magma mixing in Villarrica’s eruptive products im-  
560 plies complex magma dynamics involving multiple variably-evolved reservoirs. These may  
561 be intermittently connected and tapped prior to eruption resulting in the variable crys-  
562 tal cargoes of eruptive deposits.

### 6.3 Linking Crystal Cargo and Whole-Rock Composition to Eruptive Behavior

The complex temporal trends in the compositions of erupted crystal cargoes show strong correlations with both whole-rock composition and eruptive style. There is a stark contrast between the composition of crystal cargoes of historic eruptions and prehistoric eruptions (Figure 6). Generally, the crystal cargoes of historic eruptions contain a smaller variety of crystal compositions, this is especially pronounced for feldspar and clinopyroxene compositions. This disparity strongly correlates with whole-rock compositions (Figure 6d): historic eruptions have average bulk SiO<sub>2</sub> and MgO contents of 54 and 5 wt%, respectively, whereas prehistoric eruptions range from 54–65 wt% SiO<sub>2</sub> and 1–5 wt% MgO. Both the composition of erupted crystal cargoes and whole-rock compositions strongly correlate with eruptive style: the most differentiated eruptive deposits contain the more variable crystal cargoes and are the most explosive and high-volume.

#### 6.3.1 *Dacitic Dome*

The Dacitic Dome (c.a. 95 ka) is the most differentiated of Villarrica's products analyzed to date, with substantially higher bulk SiO<sub>2</sub> content than any subsequent eruption (65 wt% vs. 55 wt%, Figure 1). However the magma that formed the Dacitic Dome is almost certainly a mix of evolved and more primitive magmas (e.g., Eichelberger et al., 2006; Reubi & Blundy, 2009), supported by textural observations described above (Lohmar, 2008). The dacitic composition may have formed from mafic magmas ascending through evolved mushes (e.g., Reubi & Blundy, 2009) or from differentiated melts ascending through mafic mushes (e.g., Kent et al., 2010). Of the three eruptions that contain it, the crystal cargo of the Dacitic Dome contains the highest proportion of An-poor plagioclase (Pl<sub>4</sub>, Figure 6b), along with its high bulk-SiO<sub>2</sub> content.

#### 6.3.2 *The Licán and Pucón Mafic Ignimbrites*

The Licán (ca. 14 ka) and Pucón (ca. 3.7 ka) mafic ignimbrites are deposits from the two most explosive, high-volume eruptions at Villarrica (Lohmar et al., 2012; Silva Paredas, 2008). Both have high, but variable, bulk-SiO<sub>2</sub> contents (Figure 6d) compared to historic eruptions. They are also the last two eruptions whose crystal cargoes contain the evolved Pl<sub>4</sub>. Their whole-rock chemistry correlates with the proportion of Pl<sub>4</sub> in their

593 crystal cargoes: the Licán has lower MgO and slightly higher SiO<sub>2</sub> than the Pucón, and  
594 has a higher proportion of Pl<sub>4</sub> (Figure 6b,d).

595 Rhyolite-MELTS models show that Pl<sub>4</sub> likely crystallized from an evolved melt (ca.  
596 60 wt% SiO<sub>2</sub>), after substantial differentiation via crystal fractionation, resulting in a  
597 bulk crystal fraction of at least 50%. The eruption of a reservoir with such a high crys-  
598 tal fraction requires liberation via mush disaggregation to reduce its viscosity (references).  
599 This may result from a combination of chemical or thermal mixing, and/or volatile flux-  
600 ing from an incoming more primitive basaltic melt (e.g Bachmann & Bergantz, 2006; Bergantz  
601 et al., 2015; Bouvet de Maisonneuve et al., 2012; Pistone et al., 2017; Zellmer et al., 2016).  
602 Upon mixing with the primitive magma, plagioclase crystals from the evolved reservoir  
603 would become reversely-zoned, with low-An cores and higher-An rims. In turn, prim-  
604 itive plagioclase carried by this primitive melt would grow low-An rims upon mixing (as  
605 suggested in Lohmar, 2008; Lohmar et al., 2012). Therefore mixing between an evolved  
606 and primitive magma explains how Pl<sub>4</sub> can exist as cores, intermediates, and rims (Fig-  
607 ure 5).

608 The correlation of whole-rock compositions with the proportion of low-An Pl<sub>4</sub> in  
609 erupted crystal cargoes, combined with textural data and thermodynamic modeling, sup-  
610 ports the triggering of these mafic-ignimbrite generating eruptions via destabilization of  
611 a differentiated (dacitic) mush by influx of primitive magma.

### 612 ***6.3.3 The March 2015 Fire Fountain***

613 In contrast to the ignimbrite-forming eruptions, historic eruptions have been dom-  
614 inated by effusive activity, punctuated by fire fountaining which appears to be related  
615 to lahar generation (e.g., 1908, 1948-49, 1963, 1964 1971 and 2015, (Lara & Clavero, 2004)).  
616 The paroxysmal eruption of March 2015 is significant in that it was the most intense his-  
617 toric eruption at Villarrica, producing a fire fountain that was 1.5 km in height but lasted  
618 just thirty minutes (Romero et al., 2018). The composition of olivine erupted in 2015  
619 are more varied than all other historic eruptions (Figure 6), in contrast with homoge-  
620 neous plagioclase, consisting only of cluster Pl<sub>3</sub> and few clinopyroxene crystals. This im-  
621 plies that primitive magma accumulated olivine (and minor clinopyroxene) antecrysts  
622 as it ascended through the magmatic system. Plagioclase may have formed in response  
623 to degassing upon ascent (as in Blundy et al., 2006). The low-SiO<sub>2</sub> and high-MgO bulk

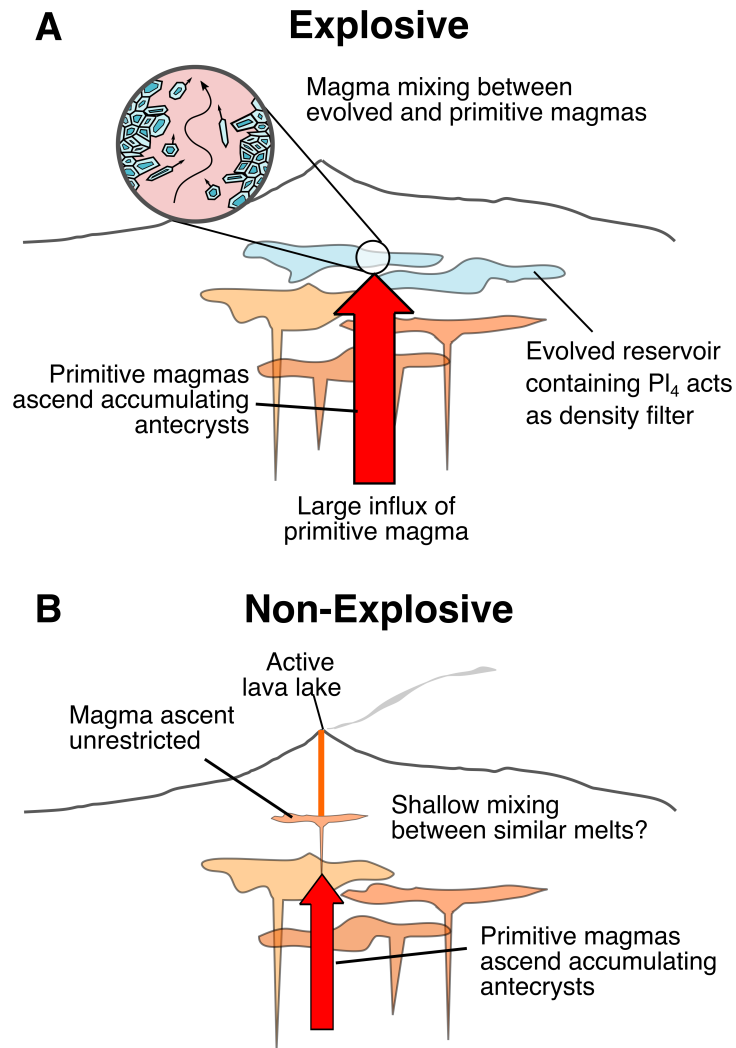


**Figure 8.** Conceptual model for Villarrica's magmatic system prior to **A.** an explosive, ignimbrite-forming eruption and **B.** a non-explosive historic eruption.

624 composition of erupted spatter suggests that the intensity of the eruption is unlikely to  
 625 be caused by the same mechanism as the mafic ignimbrites. Instead high primary volatile  
 626 contents likely drove fast magma ascent, resulting in the vigorous fountaining behavior  
 627 (Allison et al., 2021; Barth et al., 2019; La Spina et al., 2021).

#### 628 **6.4 A Model for Generating Explosive Eruptions at Villarrica Volcano**

629 The eruption of the Dacitic Dome (ca. 95 ka) demonstrates that evolved portions  
 630 of Villarrica's magmatic system existed prior to the most explosive post-glacial eruptions  
 631 known at Villarrica, the Licán ignimbrite. Therefore portions of Villarrica's magmatic

632 system were differentiated beyond the typical whole rock compositions of erupted his-  
633 toric products (Figure 1). The existence of this evolved (dacitic) reservoir has implica-  
634 tions for magma dynamics. It has been shown that felsic mushes are sufficiently viscous  
635 that they are non eruptible (Marsh, 2002; Sparks & Marshall, 1986). In combination with  
636 their low relative density, they can act as a density filter, preventing more dense mafic  
637 melts from ascending to the surface (Kent et al., 2010). Therefore the establishment of  
638 a significant volume of evolved mush within the magmatic system could dampen the erup-  
639 tion of mafic magma and increase the overall volume of evolved melt until a sufficiently  
640 large volume of ascending primitive melt is able to destabilize it (Sparks & Marshall, 1986).

641 The eruption of large-volume eruptive deposits, such as Licán and Pucón ignimbrites,  
642 requires significant volumes of mobile magma to exist within the magmatic system (Druitt  
643 & Sparks, 1984). If the majority of Villarrica’s magmatic system is composed of near-  
644 solidus mush (as implied by the TCMS model), this would require a large volume of magma  
645 to destabilize it (Marsh, 2002; Sparks & Marshall, 1986). The composition of minerals  
646 and melt inclusions at Villarrica (Ol<sub>1</sub> and Pl<sub>1</sub>, Table 2) suggest primitive magmas were  
647 present within its system (Pioli et al., 2015). Therefore we propose that the trigger of  
648 the Licán and Pucón ignimbrites was a large influx of primitive magma mixing with an  
649 evolved reservoir (Figure 8a). The remnants of the mush that this primitive magma in-  
650 teracted with is shown by the presence of evolved plagioclase, Pl<sub>4</sub> in both ignimbrites’  
651 crystal cargoes. In the case of the Licán ignimbrite, the trigger may have been magni-  
652 fied by widespread deglaciation in the Southern Andes around 14 ka ago, altering the  
653 stress state of the crust to facilitate magma ascent (e.g., Jellinek et al., 2004; Rawson  
654 et al., 2016; Watt et al., 2013; Wilson & Russell, 2020). After the eruption of the Licán  
655 ignimbrite, another evolved reservoir of similar composition likely formed over a period  
656 of ca. 10 ka. The existence of an evolved reservoir prior to the Pucón Ignimbrite (ca. 3.7  
657 ka) is suggested by a Pre-Pucón pyroclastic surge deposit Lohmar (2008), which contains  
658 a large proportion of evolved (63 wt% SiO<sub>2</sub>) pumice. The Pucón ignimbrite forming erup-  
659 tion may then have been triggered in a similar fashion to the Licán eruption, i.e. desta-  
660 bilization of an evolved reservoir by an influx of primitive magma.

661 These evolved reservoirs were likely depleted by mixing with primitive magma prior  
662 to the ignimbrite-forming eruptions as subsequently erupted crystal cargoes (3.7 ka to  
663 present) contain no trace of Pl<sub>4</sub> (Figure 6). Without the density filter provided by the  
664 evolved reservoirs, the most recently erupted magmas have been able to ascend through

Villarrica's magmatic system faster, perhaps only mixing in the shallowest parts, resulting in less differentiated erupted compositions (Figure 8b). The absence of mixing between highly differentiated and primitive compositions results in substantially lower explosivity. Instead recent lava fountaining is likely driven by rapid ascent, enabled by high volatile-contents (e.g., the March 2015 eruption). The near continuous activity at Villarrica's lava lake demonstrates the ability of magma to ascend relatively unhindered through the magmatic system. Absence of activity at the summit and/or the eruption of crystals in equilibrium with differentiated melt compositions (e.g., Pl<sub>4</sub>) may signal the onset of evolved reservoir development, and signal an increased likelihood of high-volume explosive eruption occurring.

## 7 Conclusions

Use of multivariate cluster analysis has allowed us to identify previously unidentified structure in the composition of minerals erupted throughout Villarrica's eruptive history. Comparisons of identified representative compositions with >1500 Rhyolite-MELTS thermodynamic simulations show that magma processing at Villarrica takes place at a range of pressures, temperatures, water-contents, and oxygen fugacities. These thermodynamic models strongly suggest that magma storage beneath the volcano is characterized by a series of ephemerally-connected, variably-evolved mush dominated sills. Prior to eruption, magma ascends through this trans-crustal magmatic system, accumulating different antecrysts which are erupted as variable crystal cargoes.

We have identified temporal trends in the composition of erupted crystal cargoes that correlate with trends in whole-rock composition and eruption style. We propose that prior to high-volume, ignimbrite-forming explosive mafic eruptions (the Licán and Pucón ignimbrites) much of Villarrica's volcanic system had differentiated by fractional crystallization. These evolved reservoirs acted as density filters, suppressing the eruption of small volumes of primitive magma. Only when a sufficiently-large influx of primitive magma entered the system was this evolved portion destabilized. Extensive magma mixing ensued, producing the complex textures observed by past studies, and resulting in the relatively primitive, basaltic-andesite compositions of the two ignimbrites. The only remnants of the evolved reservoir are low-anorthite plagioclase which is present as both cores and rims of more primitive crystals.

696 The absence of an evolved reservoirs, after these high-volume explosive eruptions,  
697 explains the homogeneous, more primitive, whole-rock compositions of subsequent erup-  
698 tions. Without the density filter of the evolved reservoirs, more primitive melts ascend  
699 relatively uninhibited, mixing and degassing in the shallow subsurface before eruption.  
700 Further petrological work utilizing melt inclusion compositions, high-resolution trace-  
701 element data, and diffusion chronometry will allow further investigation of magma dy-  
702 namics at Villarrica.

### 703 **Data Availability Statement**

704 All compositional data used in the clustering analysis for this study are available  
705 in the Supplementary Material.

### 706 **Acknowledgments**

707 FOB is funded by the National Environmental Research Council (NERC) Panorama Doc-  
708 toral Training Partnership (DTP) NE/S007458/1, SKE is funded by a NERC Indepen-  
709 dent Research Fellowship (NE/R015546/1). JR is supported through a Dean's Doctoral  
710 Scholar Awards of the University of Manchester and NSFGE0-NE0C-funded project Dis-  
711 Eqm (NE/N018575/1) and V-PLUS projects. All authors declare that the research was  
712 conducted in the absence of any commercial or financial relationships that could be con-  
713 strued as a potential conflict of interest. The authors would like to thank Silke Lohmar  
714 for facilitating access to compositional data.

715 **References**

- 716 Aitchison, J. (1986). *The statistical analysis of compositional data*. London ; New  
 717 York: Chapman and Hall.
- 718 Allison, C. M., Roggensack, K., & Clarke, A. B. (2021, December). Highly explosive  
 719 basaltic eruptions driven by CO<sub>2</sub> exsolution. *Nature Communications*, *12*(1),  
 720 217. doi: 10.1038/s41467-020-20354-2
- 721 Annen, C., Blundy, J. D., Leuthold, J., & Sparks, R. S. J. (2015). Construction  
 722 and evolution of igneous bodies: Towards an integrated perspective of crustal  
 723 magmatism. *Lithos*, *230*, 206–221. doi: 10.1016/j.lithos.2015.05.008
- 724 Annen, C., Blundy, J. D., & Sparks, R. S. J. (2006). The Genesis of Intermediate  
 725 and Silicic Magmas in Deep Crustal Hot Zones. *Journal of Petrology*, *47*(3),  
 726 505–539. doi: 10.1093/petrology/egi084
- 727 Bachmann, O., & Bergantz, G. W. (2006, January). Gas percolation in upper-  
 728 crustal silicic crystal mushes as a mechanism for upward heat advection  
 729 and rejuvenation of near-solidus magma bodies. *Journal of Volcanology and  
 730 Geothermal Research*, *149*(1-2), 85–102. doi: 10.1016/j.jvolgeores.2005.06.002
- 731 Barette, F., Poppe, S., Smets, B., Benbakkar, M., & Kervyn, M. (2017). Spatial  
 732 variation of volcanic rock geochemistry in the Virunga Volcanic Province: Sta-  
 733 tistical analysis of an integrated database. *Journal of African Earth Sciences*,  
 734 *134*, 888–903. doi: 10.1016/j.jafrearsci.2016.09.018
- 735 Barth, A., Newcombe, M., Plank, T., Gonnermann, H., Hajimirza, S., Soto, G. J.,  
 736 ... Hauri, E. (2019, December). Magma decompression rate correlates  
 737 with explosivity at basaltic volcanoes — Constraints from water diffusion  
 738 in olivine. *Journal of Volcanology and Geothermal Research*, *387*, 106664. doi:  
 739 10.1016/j.jvolgeores.2019.106664
- 740 Baxter, M. J., Beardah, C. C., Cool, H. E. M., & Jackson, C. M. (2005). Compo-  
 741 sitional Data Analysis of Some Alkaline Glasses. *Mathematical Geology*, *37*(2),  
 742 183–196. doi: 10.1007/s11004-005-1308-3
- 743 Bergantz, G. W., Schleicher, J. M., & Burgisser, A. (2015). Open-system dynam-  
 744 ics and mixing in magma mushes. *Nature Geoscience*, *8*(10), 793–796. doi: 10  
 745 .1038/ngeo2534
- 746 Blundy, J., Cashman, K., & Humphreys, M. (2006, September). Magma heating  
 747 by decompression-driven crystallization beneath andesite volcanoes. *Nature*,



- 748 443(7107), 76–80. doi: 10.1038/nature05100
- 749 Bouvet de Maisonneuve, C., Dungan, M., Bachmann, O., & Burgisser, A. (2012).  
750 Insights into shallow magma storage and crystallization at Volcán Llaima (An-  
751 dean Southern Volcanic Zone, Chile). *Journal of Volcanology and Geothermal*  
752 *Research*, 211-212, 76–91. doi: 10.1016/j.jvolgeores.2011.09.010
- 753 Caricchi, L., Petrelli, M., Bali, E., Sheldrake, T., Pioli, L., & Simpson, G. (2020).  
754 A Data Driven Approach to Investigate the Chemical Variability of Clinopy-  
755 roxenes From the 2014–2015 Holuhraun–Bárdarbunga Eruption (Iceland).  
756 *Frontiers in Earth Science*, 8, 18. doi: 10.3389/feart.2020.00018
- 757 Carmichael, I. S. E. (1991, January). The redox states of basic and silicic magmas:  
758 A reflection of their source regions? *Contributions to Mineralogy and Petrol-*  
759 *ogy*, 106(2), 129–141. doi: 10.1007/BF00306429
- 760 Cashman, K. V., Sparks, R. S. J., & Blundy, J. D. (2017). Vertically extensive  
761 and unstable magmatic systems: A unified view of igneous processes. *Science*,  
762 355(6331), eaag3055. doi: 10.1126/science.aag3055
- 763 Cembrano, J., & Lara, L. (2009, June). The link between volcanism and tectonics  
764 in the southern volcanic zone of the Chilean Andes: A review. *Tectonophysics*,  
765 471(1-2), 96–113. doi: 10.1016/j.tecto.2009.02.038
- 766 Chayes, F. (1971). *Ratio correlation: a manual for students of petrology and geo-*  
767 *chemistry*. University of Chicago Press.
- 768 Cheng, L., Costa, F., & Carniel, R. (2017, September). Unraveling the presence  
769 of multiple plagioclase populations and identification of representative two-  
770 dimensional sections using a statistical and numerical approach. *American*  
771 *Mineralogist*, 102(9), 1894–1905. doi: 10.2138/am-2017-5929CCBYNCND
- 772 Chiasera, B., & Cortés, J. A. (2011). Predictive regions for geochemical compo-  
773 sitional data of volcanic systems. *Journal of Volcanology and Geothermal Re-*  
774 *search*, 207(3-4), 83–92. doi: 10.1016/j.jvolgeores.2011.07.009
- 775 Clavero-Ribes, J. (1996). *Ignimbritas andesítico-basálticas postglaciales del volcán*  
776 *villarrica, andes del sur (39° 25's)* (Unpublished master’s thesis). Universidad  
777 de Chile, Chile.
- 778 Cooper, K. M., & Kent, A. J. R. (2014). Rapid remobilization of magmatic crystals  
779 kept in cold storage. *Nature*, 506(7489), 480–483. doi: 10.1038/nature12991
- 780 Corsaro, R. A., Falsaperla, S., & Langer, H. (2013). Geochemical pattern classi-

- 781       fication of recent volcanic products from Mt. Etna, Italy, based on Kohonen  
782       maps and fuzzy clustering. *International Journal of Earth Sciences*, 102(4),  
783       1151–1164. doi: 10.1007/s00531-012-0851-7
- 784       Cortés, J. A. (2009). On the Harker Variation Diagrams; A Comment on “The Sta-  
785       tistical Analysis of Compositional Data. Where Are We and Where Should We  
786       Be Heading?” by Aitchison and Egozcue (2005). *Mathematical Geosciences*,  
787       41(7), 817–828. doi: 10.1007/s11004-009-9222-8
- 788       Cortés, J. A., Palma, J. L., & Wilson, M. (2007). Deciphering magma mixing: The  
789       application of cluster analysis to the mineral chemistry of crystal populations.  
790       *Journal of Volcanology and Geothermal Research*, 165(3-4), 163–188. doi:  
791       10.1016/j.jvolgeores.2007.05.018
- 792       Costantini, L., Pioli, L., Bonadonna, C., Clavero, J., & Longchamp, C. (2011). A  
793       Late Holocene explosive mafic eruption of Villarrica volcano, Southern Andes:  
794       The Chaimilla deposit. *Journal of Volcanology and Geothermal Research*,  
795       200(3-4), 143–158. doi: 10.1016/j.jvolgeores.2010.12.010
- 796       Delgado, F., Pritchard, M. E., Ebmeier, S., González, P., & Lara, L. (2017).  
797       Recent unrest (2002–2015) imaged by space geodesy at the highest risk  
798       Chilean volcanoes: Villarrica, Llaima, and Calbuco (Southern Andes).  
799       *Journal of Volcanology and Geothermal Research*, 344, 270–288. doi:  
800       10.1016/j.jvolgeores.2017.05.020
- 801       Droop, G. T. R. (1987). A general equation for estimating Fe<sup>3+</sup> concentra-  
802       tions in ferromagnesian silicates and oxides from microprobe analyses, us-  
803       ing stoichiometric criteria. *Mineralogical Magazine*, 51(361), 431–435. doi:  
804       10.1180/minmag.1987.051.361.10
- 805       Druitt, T. H., & Sparks, R. S. J. (1984, August). On the formation of calderas dur-  
806       ing ignimbrite eruptions. *Nature*, 310(5979), 679–681. doi: 10.1038/310679a0
- 807       Ebmeier, S. K., Andrews, B. J., Araya, M. C., Arnold, D. W. D., Biggs, J., Cooper,  
808       C., . . . Williamson, J. L. (2018, December). Synthesis of global satellite ob-  
809       servations of magmatic and volcanic deformation: Implications for volcano  
810       monitoring & the lateral extent of magmatic domains. *Journal of Applied*  
811       *Volcanology*, 7(1), 2. doi: 10.1186/s13617-018-0071-3
- 812       Egozcue, J. J., Pawlowsky-Glahn, V., Mateu-Figueras, G., & Barcelo-Vidal, C.  
813       (2003). Isometric Logratio Transformations for Compositional Data Analysis.

- 814 *Mathematical Geology*, 22.
- 815 Eichelberger, J. C., Izbekov, P. E., & Browne, B. L. (2006, March). Bulk chemi-  
 816 cal trends at arc volcanoes are not liquid lines of descent. *Lithos*, 87(1-2), 135–  
 817 154. doi: 10.1016/j.lithos.2005.05.006
- 818 Feig, S. T., Koepke, J., & Snow, J. E. (2010). Effect of oxygen fugacity and water on  
 819 phase equilibria of a hydrous tholeiitic basalt. *Contributions to Mineralogy and*  
 820 *Petrology*, 160(4), 551–568. doi: 10.1007/s00410-010-0493-3
- 821 Filzmoser, P., & Hron, K. (2008). Outlier Detection for Compositional Data Using  
 822 Robust Methods. *Mathematical Geosciences*, 40(3), 233–248. doi: 10.1007/  
 823 s11004-007-9141-5
- 824 Fry, J. M., Fry, T. R. L., & McLaren, K. R. (2000). Compositional data analysis  
 825 and zeros in micro data. *Applied Economics*, 32(8), 953–959. doi: 10.1080/  
 826 000368400322002
- 827 Gainsforth, Z., Butterworth, A. L., Stodolna, J., Westphal, A. J., Huss, G. R., Na-  
 828 gashima, K., . . . Simionovici, A. S. (2015). Constraints on the formation  
 829 environment of two chondrule-like igneous particles from comet 81P/Wild 2.  
 830 *Meteoritics & Planetary Science*, 50(5), 976–1004. doi: 10.1111/maps.12445
- 831 Gavrilenko, M., Herzberg, C., Vidito, C., Carr, M. J., Tenner, T., & Ozerov, A.  
 832 (2016). A Calcium-in-Olivine Geothermometer and its Application to Sub-  
 833 duction Zone Magmatism. *Journal of Petrology*, 57(9), 1811–1832. doi:  
 834 10.1093/petrology/egw062
- 835 Ghiorso, M. S., & Gualda, G. A. R. (2015). An H<sub>2</sub>O–CO<sub>2</sub> mixed fluid saturation  
 836 model compatible with rhyolite-MELTS. *Contributions to Mineralogy and*  
 837 *Petrology*, 169(6), 53. doi: 10.1007/s00410-015-1141-8
- 838 Ginibre, C., & Wörner, G. (2007). Variable parent magmas and recharge regimes of  
 839 the Parinacota magma system (N. Chile) revealed by Fe, Mg and Sr zoning in  
 840 plagioclase. *Lithos*, 98(1-4), 118–140. doi: 10.1016/j.lithos.2007.03.004
- 841 Greenacre, M. (2019). Variable Selection in Compositional Data Analysis Using  
 842 Pairwise Logratios. *Mathematical Geosciences*, 51(5), 649–682. doi: 10.1007/  
 843 s11004-018-9754-x
- 844 Greenacre, M., & Lewi, P. (2009). Distributional Equivalence and Subcomposi-  
 845 tional Coherence in the Analysis of Compositional Data, Contingency Tables  
 846 and Ratio-Scale Measurements. *Journal of Classification*, 26(1), 29–54. doi:

- 847 10.1007/s00357-009-9027-y
- 848 Gualda, G. A. R., Ghiorso, M. S., Lemons, R. V., & Carley, T. L. (2012). Rhyolite-  
849 MELTS: A Modified Calibration of MELTS Optimized for Silica-rich, Fluid-  
850 bearing Magmatic Systems. *Journal of Petrology*, *53*(5), 875–890. doi:  
851 10.1093/petrology/egr080
- 852 Hamada, M., Iwamori, H., Brandl, P. A., Ushikubo, T., Shimizu, K., Ito, M., ...  
853 Savov, I. P. (2020). Temporal Evolution of Proto-Izu–Bonin–Mariana  
854 Arc Volcanism over 10 Myr: Constraints from Statistical Analysis of Melt  
855 Inclusion Compositions. *Journal of Petrology*, *61*(1), ega022. doi:  
856 10.1093/petrology/egaa022
- 857 Henze, N., & Zirkler, B. (1990). A class of invariant consistent tests for multivariate  
858 normality. *Communications in statistics-Theory and Methods*, *19*(10), 3595–  
859 3617.
- 860 Hickey-Vargas, R., Roa, H. M., Escobar, L. L., & Frey, F. A. (1989). Geochem-  
861 ical variations in Andean basaltic and silicic lavas from the Villarrica-Lanin  
862 volcanic chain (39.5° S): An evaluation of source heterogeneity, fractional crys-  
863 tallization and crustal assimilation. *Contributions to Mineralogy and Petrology*,  
864 *103*(3), 361–386. doi: 10.1007/BF00402922
- 865 Hickey-Vargas, R., Sun, M., & Holbik, S. (2016). Geochemistry of basalts from small  
866 eruptive centers near Villarrica stratovolcano, Chile: Evidence for lithospheric  
867 mantle components in continental arc magmas. *Geochimica et Cosmochimica*  
868 *Acta*, *185*, 358–382. doi: 10.1016/j.gca.2016.03.033
- 869 Hildreth, W., & Moorbath, S. (1988, April). Crustal contributions to arc magma-  
870 tism in the Andes of Central Chile. *Contributions to Mineralogy and Petrology*,  
871 *98*(4), 455–489. doi: 10.1007/BF00372365
- 872 Jellinek, A. M., Manga, M., & Saar, M. O. (2004, September). Did melting glaciers  
873 cause volcanic eruptions in eastern California? Probing the mechanics of dike  
874 formation: VOLCANISM AND DEGLACIATION. *Journal of Geophysical*  
875 *Research: Solid Earth*, *109*(B9), n/a-n/a. doi: 10.1029/2004JB002978
- 876 Jerram, D. A., & Martin, V. M. (2008). Understanding crystal populations and their  
877 significance through the magma plumbing system. *Geological Society, London,*  
878 *Special Publications*, *304*(1), 133–148. doi: 10.1144/SP304.7
- 879 Kamenetsky, V. S., Elburg, M., Arculus, R., & Thomas, R. (2006). Mag-

- 880 matic origin of low-Ca olivine in subduction-related magmas: Co-existence  
 881 of contrasting magmas. *Chemical Geology*, 233(3-4), 346–357. doi:  
 882 10.1016/j.chemgeo.2006.03.010
- 883 Kapinos, G., Montahaei, M., Meqbel, N., & Brasse, H. (2016). Three-dimensional  
 884 electrical resistivity image of the South-Central Chilean subduction zone.  
 885 *Tectonophysics*, 666, 76–89. doi: 10.1016/j.tecto.2015.10.016
- 886 Kent, A. J. R., Darr, C., Koleszar, A. M., Salisbury, M. J., & Cooper, K. M. (2010).  
 887 Preferential eruption of andesitic magmas through recharge filtering. *Nature*  
 888 *Geoscience*, 3(9), 631–636. doi: 10.1038/ngeo924
- 889 Kuritani, T., Yamaguchi, A., Fukumitsu, S., Nakagawa, M., Matsumoto, A., &  
 890 Yokoyama, T. (2018). Magma Plumbing System at Izu-Oshima Volcano,  
 891 Japan: Constraints From Petrological and Geochemical Analyses. *Frontiers in*  
 892 *Earth Science*, 6, 178. doi: 10.3389/feart.2018.00178
- 893 Lara, L. E., & Clavero, J. (2004). *Villarrica Volcano (39.5 S), Southern Andes,*  
 894 *Chile* (Vol. Bulletin 61).
- 895 La Spina, G., Arzilli, F., Llewellyn, E. W., Burton, M. R., Clarke, A. B., de' Michieli  
 896 Vitturi, M., ... Mader, H. M. (2021, January). Explosivity of basaltic lava  
 897 fountains is controlled by magma rheology, ascent rate and outgassing. *Earth*  
 898 *and Planetary Science Letters*, 553, 116658. doi: 10.1016/j.epsl.2020.116658
- 899 Le Bas, M. J., Maitre, R. W. L., Streckeisen, A., Zanettin, B., & IUGS Subcommis-  
 900 sion on the Systematics of Igneous Rocks. (1986). A Chemical Classification of  
 901 Volcanic Rocks Based on the Total Alkali-Silica Diagram. *Journal of Petrology*,  
 902 27(3), 745–750. doi: 10.1093/petrology/27.3.745
- 903 Lerner, A. H., O'Hara, D., Karlstrom, L., Ebmeier, S. K., Anderson, K. R., & Hur-  
 904 witz, S. (2020, July). The Prevalence and Significance of Offset Magma  
 905 Reservoirs at Arc Volcanoes. *Geophysical Research Letters*, 47(14). doi:  
 906 10.1029/2020GL087856
- 907 Lindsley, D. H., & Frost, B. R. (1992, October). Equilibria among Fe-Ti oxides, py-  
 908 roxenes, olivine, and quartz: Part I. Theory. *American Mineralogist*, 77(9-10),  
 909 987–1003.
- 910 Liu, E. J., Cashman, K. V., Miller, E., Moore, H., Edmonds, M., Kunz, B. E., ...  
 911 Chigna, G. (2020). Petrologic monitoring at Volcán de Fuego, Guatemala.  
 912 *Journal of Volcanology and Geothermal Research*, 405, 107044. doi:

- 913 10.1016/j.jvolgeores.2020.107044
- 914 Liu, X., Wang, W., Pei, Y., & Yu, P. (2020). A knowledge-driven way to in-  
915 terpret the isometric log-ratio transformation and mixture distributions of  
916 geochemical data. *Journal of Geochemical Exploration*, 210, 106417. doi:  
917 10.1016/j.gexplo.2019.106417
- 918 Lohmar, S. (2008). *Petrologia de las Ignimbritas Licán y Pucón (Volcan Villarrica)*  
919 *y Curacautin (Volcan LLaima) en los Andes del sur de Chile* (Unpublished  
920 doctoral dissertation). Universidad de Chile, Chile.
- 921 Lohmar, S., Parada, M., Gutiérrez, F., Robin, C., & Gerbe, M. C. (2012). Min-  
922 eralogical and numerical approaches to establish the pre-eruptive conditions  
923 of the mafic Licán Ignimbrite, Villarrica Volcano (Chilean Southern An-  
924 des). *Journal of Volcanology and Geothermal Research*, 235-236, 55–69. doi:  
925 10.1016/j.jvolgeores.2012.05.006
- 926 Loucks, R. R. (1996, October). A precise olivine-augite Mg-Fe-exchange geother-  
927 mometer. *Contributions to Mineralogy and Petrology*, 125(2-3), 140–150. doi:  
928 10.1007/s004100050211
- 929 Mahalanobis, P. C. (1936). On the generalized distance in statistics. *National Insti-*  
930 *tute of Science of India*, 2, 49–55.
- 931 Marsh, B. D. (2002, June). On bimodal differentiation by solidification front insta-  
932 bility in basaltic magmas, part 1: Basic mechanics. *Geochimica et Cosmochim-*  
933 *ica Acta*, 66(12), 2211–2229. doi: 10.1016/S0016-7037(02)00905-5
- 934 Martín-Fernández, J. A., Barceló-Vidal, C., & Pawlowsky-Glahn, V. (2000). Zero  
935 Replacement in Compositional Data Sets. In H.-H. Bock et al. (Eds.), *Data*  
936 *Analysis, Classification, and Related Methods* (pp. 155–160). Berlin, Heidel-  
937 berg: Springer Berlin Heidelberg. doi: 10.1007/978-3-642-59789-3\_25
- 938 McCurry, M., Chadwick, J., Wright, K., Smith, R., & Ford, M. (2004). Preliminary  
939 la/icp-ms and epma examination of dacite enclaves and melt inclusions in phe-  
940 nocrysts from basaltic andesite pyroclasts from the pucón ignimbrite, volcán  
941 villarrica, southern andean volcanic zone: Implications for mafic ignimbrite  
942 volcanism..
- 943 McCurry, M., & Schmidt, K. (2001). Petrology and oxygen isotope geochemistry  
944 of the pucon ignimbrite-southern andean volcanic zone, chile: Implications for  
945 genesis of mafic ignimbrites..

- 946 McGee, L. E., Brahm, R., Rowe, M. C., Handley, H. K., Morgado, E., Lara, L. E.,  
 947 ... Valdivia, P. (2017). A geochemical approach to distinguishing competing  
 948 tectono-magmatic processes preserved in small eruptive centres. *Contributions*  
 949 *to Mineralogy and Petrology*, 172(6), 44. doi: 10.1007/s00410-017-1360-2
- 950 Mollo, S., Putirka, K., Iezzi, G., Del Gaudio, P., & Scarlato, P. (2011). Pla-  
 951 gioclase–melt (dis)equilibrium due to cooling dynamics: Implications for  
 952 thermometry, barometry and hygrometry. *Lithos*, 125(1-2), 221–235. doi:  
 953 10.1016/j.lithos.2011.02.008
- 954 Moreno, H. (1993). Volcán villarrica, geología y evaluación del riesgo volcánico, re-  
 955 giones IX y x, 39 25 s. *Informe Final Proyecto FONDECYT*, 1247, 1–112.
- 956 Moreno, H., & Clavero, J. (2006). Geología del volcán Villarrica, Regiones de La  
 957 Araucanía y de Los Lagos. Carta Geológica de Chile, Serie Geología Básica,  
 958 No. 98. Servicio Nacional de Geología y Minería. Mapa Escala 1:50,000. Santi-  
 959 ago, Chile.
- 960 Moreno, H., Clavero, J., & Lara, L. (1994). Actividad Explosiva Postglacial del  
 961 Volcan Villarrica, Andes del Sur (39o25’S). In *7th Congreso Geológico Chileno*  
 962 (Vol. 1, pp. 329–333). Universidad de Concepcion.
- 963 Morgado, E., Parada, M., Contreras, C., Castruccio, A., Gutiérrez, F., & McGee, L.  
 964 (2015). Contrasting records from mantle to surface of Holocene lavas of two  
 965 nearby arc volcanic complexes: Caburgua-Huelemolle Small Eruptive Centers  
 966 and Villarrica Volcano, Southern Chile. *Journal of Volcanology and Geother-  
 967 mal Research*, 306, 1–16. doi: 10.1016/j.jvolgeores.2015.09.023
- 968 Mutch, E. J. F., MacLennan, J., Shorttle, O., Edmonds, M., & Rudge, J. F. (2019).  
 969 Rapid transcrustal magma movement under Iceland. *Nature Geoscience*,  
 970 12(7), 569–574. doi: 10.1038/s41561-019-0376-9
- 971 Panjasawatwong, Y., Danyushevsky, L. V., Crawford, A. J., & Harris, K. L. (1995).  
 972 An experimental study of the effects of melt composition on plagioclase–melt  
 973 equilibria at 5 and 10 kbar: Implications for the origin of magmatic high-An  
 974 plagioclase. *Contributions to Mineralogy and Petrology*, 118(4), 420–432. doi:  
 975 10.1007/s004100050024
- 976 Pavez, M., Schill, E., Held, S., Díaz, D., & Kohl, T. (2020, August). Visualizing  
 977 preferential magmatic and geothermal fluid pathways via electric conductiv-  
 978 ity at Villarrica Volcano, S-Chile. *Journal of Volcanology and Geothermal*

- 979 *Research*, 400, 106913. doi: 10.1016/j.jvolgeores.2020.106913
- 980 Pedregosa, F., Varoquaux, G., Gramfort, A., Michel, V., Thirion, B., Grisel, O., ...  
 981 Duchesnay, É. (2011). Scikit-learn: Machine Learning in Python. *Journal of*  
 982 *Machine Learning Research*, 12(85), 2825–2830.
- 983 Petit-Breuilh, M. (2004). *La historia eruptiva de los volcanes hispanoamericanos*  
 984 *(siglos xvi al xx)*. Servicio de Publicaciones Exmo. Cabildo Insular de Lan-  
 985 zarote. Huelva, Spain.
- 986 Pichavant, M., Costa, F., Burgisser, A., Scaillet, B., Martel, C., & Poussineau, S.  
 987 (2007, September). Equilibration Scales in Silicic to Intermediate Magmas Im-  
 988 plications for Experimental Studies. *Journal of Petrology*, 48(10), 1955–1972.  
 989 doi: 10.1093/petrology/egm045
- 990 Pioli, L., Scalisi, L., Costantini, L., Di Muro, A., Bonadonna, C., & Clavero, J.  
 991 (2015). Explosive style, magma degassing and evolution in the Chaimilla erup-  
 992 tion, Villarrica volcano, Southern Andes. *Bulletin of Volcanology*, 77(11), 93.  
 993 doi: 10.1007/s00445-015-0976-1
- 994 Pistone, M., Blundy, J., & Brooker, R. A. (2017, April). Water transfer dur-  
 995 ing magma mixing events: Insights into crystal mush rejuvenation and  
 996 melt extraction processes. *American Mineralogist*, 102(4), 766–776. doi:  
 997 10.2138/am-2017-5793
- 998 Pizarro, C., Parada, M. A., Contreras, C., & Morgado, E. (2019). Cryptic magma  
 999 recharge associated with the most voluminous 20th century eruptions (1921,  
 1000 1948 and 1971) at Villarrica Volcano. *Journal of Volcanology and Geothermal*  
 1001 *Research*, 384, 48–63. doi: 10.1016/j.jvolgeores.2019.07.001
- 1002 Rawson, H., Pyle, D. M., Mather, T. A., Smith, V. C., Fontijn, K., Lachowycz,  
 1003 S. M., & Naranjo, J. A. (2016, April). The magmatic and eruptive response  
 1004 of arc volcanoes to deglaciation: Insights from southern Chile. *Geology*, 44(4),  
 1005 251–254. doi: 10.1130/G37504.1
- 1006 Reubi, O., & Blundy, J. (2009). A dearth of intermediate melts at subduction zone  
 1007 volcanoes and the petrogenesis of arc andesites. *Nature*, 461(7268), 1269–1273.  
 1008 doi: 10.1038/nature08510
- 1009 Robidoux, P., Pastén, D., Levresse, G., Diaz, G., & Paredes, D. (2021, July).  
 1010 Volatile Content Implications of Increasing Explosivity of the Strombolian  
 1011 Eruptive Style along the Fracture Opening on the NE Villarrica Flank: Mi-



- 1012 nor Eruptive Centers in the Los Nevados Group 2. *Geosciences*, 11(8). doi:  
1013 10.3390/geosciences11080309
- 1014 Romero, J. E., Vera, F., Polacci, M., Morgavi, D., Arzilli, F., Alam, M. A., ...  
1015 Keller, W. (2018). Tephra From the 3 March 2015 Sustained Column Related  
1016 to Explosive Lava Fountain Activity at Volcán Villarrica (Chile). *Frontiers in*  
1017 *Earth Science*, 6, 98. doi: 10.3389/feart.2018.00098
- 1018 Rousseeuw, P. J., & Driessen, K. V. (1999). A Fast Algorithm for the Minimum Co-  
1019 variance Determinant Estimator. *Technometrics*, 41(3), 212–223. doi: 10.1080/  
1020 00401706.1999.10485670
- 1021 Rousseeuw, P. J., & Zomeren, B. C. V. (1990). Unmasking Multivariate Out-  
1022 liers and Leverage Points. *Journal of The American Statistical Association*,  
1023 85(411), 633–639.
- 1024 Ruprecht, P., Bergantz, G. W., Cooper, K. M., & Hildreth, W. (2012). The crustal  
1025 magma storage system of volcán quizapu, chile, and the effects of magma  
1026 mixing on magma diversity. *Journal of Petrology*, 53(4), 801–840.
- 1027 Sato, M. (1978, June). Oxygen fugacity of basaltic magmas and the role of gas-  
1028 forming elements. *Geophysical Research Letters*, 5(6), 447–449. doi: 10.1029/  
1029 GL005i006p00447
- 1030 SERNAGEOMIN. (2019). *Ranking de riesgo de volcanes activos de Chile 2019*  
1031 (Tech. Rep.). SERNAGEOMIN. Retrieved from [https://www.sernageomin](https://www.sernageomin.cl/geologia)  
1032 [.cl/geologia](https://www.sernageomin.cl/geologia)
- 1033 Siebert, L., Cottrell, E., Venzke, E., & Andrews, B. (2015, January). Chapter 12 -  
1034 Earth's Volcanoes and Their Eruptions: An Overview. In H. Sigurdsson (Ed.),  
1035 *The Encyclopedia of Volcanoes (Second Edition)* (pp. 239–255). Amsterdam:  
1036 Academic Press. doi: 10.1016/B978-0-12-385938-9.00012-2
- 1037 Silva Parejas, C. (2008). *Evolution and Dynamics of the 3.6 Ka BP Pucón Erup-*  
1038 *tion of Villarrica Volcano, Chile* (Unpublished doctoral dissertation). Universi-  
1039 dad de Chile, Santiago, Chile.
- 1040 Silva Parejas, C., Druitt, T. H., Robin, C., Moreno, H., & Naranjo, J.-A. (2010).  
1041 The Holocene Pucón eruption of Volcán Villarrica, Chile: Deposit architec-  
1042 ture and eruption chronology. *Bulletin of Volcanology*, 72(6), 677–692. doi:  
1043 10.1007/s00445-010-0348-9
- 1044 Silverman, B. W. (1986). *Density estimation for statistics and data analysis*

- 1045 (No. 26). Boca Raton: Chapman & Hall/CRC.
- 1046 Singer, B. S., Dungan, M. A., & Layne, G. D. (1995). Textures and Sr, Ba, Mg, Fe,  
1047 K and Ti compositional profiles in volcanic plagioclase clues to the dynamics  
1048 of calc-alkaline magma chambers. *American Mineralogist*, *80*(7-8), 776–798.  
1049 doi: 10.2138/am-1995-7-815
- 1050 Smith, P. M., & Asimow, P. D. (2005). Adibat\_1ph: A new public front-end to the  
1051 MELTS, pMELTS, and pHMELTS models: ADIABAT\_1PH FRONT-END.  
1052 *Geochemistry, Geophysics, Geosystems*, *6*(2). doi: 10.1029/2004GC000816
- 1053 Sparks, R., & Marshall, L. (1986, September). Thermal and mechanical constraints  
1054 on mixing between mafic and silicic magmas. *Journal of Volcanology and  
1055 Geothermal Research*, *29*(1-4), 99–124. doi: 10.1016/0377-0273(86)90041-7
- 1056 Stern, C. R. (2004, December). Active Andean volcanism: Its geologic and  
1057 tectonic setting. *Revista geológica de Chile*, *31*(2). doi: 10.4067/S0716  
1058 -02082004000200001
- 1059 Streck, M. J. (2008, January). Mineral Textures and Zoning as Evidence for Open  
1060 System Processes. *Reviews in Mineralogy and Geochemistry*, *69*(1), 595–622.  
1061 doi: 10.2138/rmg.2008.69.15
- 1062 Takagi, D., Sato, H., & Nakagawa, M. (2005). Experimental study of a low-alkali  
1063 tholeiite at 1–5 kbar: Optimal condition for the crystallization of high-An pla-  
1064 gioclase in hydrous arc tholeiite. *Contributions to Mineralogy and Petrology*,  
1065 *149*(5), 527–540. doi: 10.1007/s00410-005-0666-7
- 1066 Templ, M., Filzmoser, P., & Reimann, C. (2008). Cluster analysis applied to re-  
1067 gional geochemical data: Problems and possibilities. *Applied Geochemistry*,  
1068 *23*(8), 2198–2213. doi: 10.1016/j.apgeochem.2008.03.004
- 1069 Van der Maaten, L., & Hinton, G. (2008). Visualizing data using t-SNE. *Journal of  
1070 machine learning research*, *9*(11).
- 1071 Ward, J. H. (1963). Hierarchical Grouping to Optimize an Objective Function. *Jour-  
1072 nal of The American Statistical Association*, *58*(301), 236–244.
- 1073 Waters, L. E., & Lange, R. A. (2015). An updated calibration of the plagioclase-  
1074 liquid hygrometer-thermometer applicable to basalts through rhyolites. *Ameri-  
1075 can Mineralogist*, *100*(10), 2172–2184. doi: 10.2138/am-2015-5232
- 1076 Watt, S. F., Pyle, D. M., & Mather, T. A. (2013, July). The volcanic re-  
1077 sponse to deglaciation: Evidence from glaciated arcs and a reassessment

- 1078 of global eruption records. *Earth-Science Reviews*, 122, 77–102. doi:  
1079 10.1016/j.earscirev.2013.03.007
- 1080 Wehrmann, H., Hoernle, K., Jacques, G., Garbe-Schönberg, D., Schumann, K.,  
1081 Mahlke, J., & Lara, L. E. (2014). Volatile (sulphur and chlorine), major, and  
1082 trace element geochemistry of mafic to intermediate tephros from the Chilean  
1083 Southern Volcanic Zone (33–43°S). *International Journal of Earth Sciences*,  
1084 103(7), 1945–1962. doi: 10.1007/s00531-014-1006-9
- 1085 Williams, M., Schoneveld, L., Mao, Y., Klump, J., Gosses, J., Dalton, H., ...  
1086 Barnes, S. (2020). Pyrolite: Python for geochemistry. *Journal of Open*  
1087 *Source Software*, 5(50), 2314. doi: 10.21105/joss.02314
- 1088 Williams, W. T., & Lambert, J. M. (1966). Multivariate Methods in Plant Ecol-  
1089 ogy: V. Similarity Analyses and Information-Analysis. *The Journal of Ecology*,  
1090 54(2), 427. doi: 10.2307/2257960
- 1091 Wilson, A., & Russell, J. (2020, October). Glacial pumping of a magma-charged  
1092 lithosphere: A model for glaciovolcanic causality in magmatic arcs. *Earth and*  
1093 *Planetary Science Letters*, 548, 116500. doi: 10.1016/j.epsl.2020.116500
- 1094 Wishart, D. (1969). Numerical Classification Method for deriving Natural Classes.  
1095 *Nature*, 221(5175), 97–98. doi: 10.1038/221097a0
- 1096 Witter, J. B., Kress, V. C., Delmelle, P., & Stix, J. (2004). Volatile degassing,  
1097 petrology, and magma dynamics of the Villarrica Lava Lake, Southern Chile.  
1098 *Journal of Volcanology and Geothermal Research*, 134(4), 303–337. doi:  
1099 10.1016/j.jvolgeores.2004.03.002
- 1100 Zajacz, Z., & Halter, W. (2007). LA-ICPMS analyses of silicate melt inclusions  
1101 in co-precipitated minerals: Quantification, data analysis and mineral/melt  
1102 partitioning. *Geochimica et Cosmochimica Acta*, 71(4), 1021–1040. doi:  
1103 10.1016/j.gca.2006.11.001
- 1104 Zajacz, Z., & Halter, W. (2009). Copper transport by high temperature, sulfur-rich  
1105 magmatic vapor: Evidence from silicate melt and vapor inclusions in a basaltic  
1106 andesite from the Villarrica volcano (Chile). *Earth and Planetary Science*  
1107 *Letters*, 282(1-4), 115–121. doi: 10.1016/j.epsl.2009.03.006
- 1108 Zellmer, G. F., Pistone, M., Iizuka, Y., Andrews, B. J., Gómez-Tuena, A., Straub,  
1109 S. M., & Cottrell, E. (2016, November). Petrogenesis of antecryst-bearing arc  
1110 basalts from the Trans-Mexican Volcanic Belt: Insights into along-arc varia-

1111 tions in magma-mush ponding depths, H<sub>2</sub>O contents, and surface heat flux.  
1112 *American Mineralogist*, 101(11), 2405–2422. doi: 10.2138/am-2016-5701